TELECAT project

New Teleseismic Catalogue for NOA – Bridging the gap

Report # 2

Fevronia Gkika (1) and Jens Havskov (2)

(1) Institute of Geodynamics, National Observatory of Athens, Greece
(2) Department of Geoscience, University of Bergen, Norway

Emails:gkika@noa.gr , Jens.Havskov@uib.no

08/05/2026

Notice

The material in this report formed the basis of the published scientific paper:

Gkika, F., Havskov, J., & Evangelidis, C. P. (2026). Teleseismic Data, Contribution from Greece. *Seismological Research Letters*. https://doi.org/10.1785/0220250254

This document represents the author's technical report version and is provided for academic dissemination and research accessibility. The final published version may differ from this manuscript in formatting, corrected values, magnitudes, calibration, and reviewed interpretations.

For the final peer-reviewed and corrected version of the work, readers should consult the published article referenced above.

Introduction

The Institute of Geodynamics of the National Observatory of Athens (GI-NOA) has provided consistent reports on teleseismic events, as documented in printed bulletins. GI-NOA regularly released monthly bulletins at least up to 2002 that included a section of teleseismic event information predominantly relying on a dozen Greek seismic stations (printed monthly Bulletins by NOA-GI, 1950 - 2002). Following that period, the GI-NOA teleseismic analyses reports are only sent to the ISC and no printed bulletins were made. This time period coincided with the stations passing from analog to digital and the later unification of the network in 2008. However, it remained uncertain whether all teleseismic events were processed, and the precise duration of discontinuation for these analyses is unknown. Through an extensive search into the ISC database in both bulletins and the Greek stations phase reports, it has been verified that reports on teleseismic events by the ATH agency (same as NOA), as documented by the ISC under the National Observatory of Athens (NOA), extends up to the year 2010.

Therefore, a notable shift occurred sometime in or after 2011, as the Institute ceased reporting teleseismic phases to the ISC. Subsequently, the sole contributor from the Greek side became THE agency (Department of Geophysics, Aristotle University of Thessaloniki), which continued reporting first arrivals from teleseismic events of the same unified network as used by NOA. In cases where a foreign agency exclusively reports teleseismic phases from Greek stations for events not analyzed by a Greek agency, it typically relies on a limited number of available stations. As we shall see later, THE only reported P-phases with no magnitudes and location information. This study aims to address the information gap resulting from the discontinuation of teleseismic event reporting by the Institute (NOA). Despite THE having reported continuously since 2011, we have observed that there are gaps in their reporting, particularly with respect to 2012-2021 and we intend to fill those gaps. The primary objective is to have a complete data base of large events as recorded with the Greek network as well as to contribute to the global solutions, especially in the context of large seismic events. We intend to extract as much available information as possible, laying the foundation for future research activities. In the current study, we intend to evaluate the Greek network capability to locate global events. We will calculate the normally

used global magnitude mb and Ms (for 2019 only) as well as the less used broad band magnitudes mB and MS. The magnitudes will be compared to ISC determined magnitudes to find if any discrepancies from the global values. Also local magnitude station anomalies will be studied.

The intention for NOA is to continue to report teleseismic data and our study will also help to set procedures for the teleseismic operation as described in the following sections. Some of the text, particular some technical parts, are repeated from the first technical report (Gkika and Havskov 2023). These sections will be quoted.

Station selection from the Hellenic Unified Seismic Network

"The Hellenic Unified Seismic Network (HUSN) is an extensive seismic network comprising almost 150 stations nationwide which is in continuous operation with real-time data transmission. Two-thirds of the stations are equipped with triaxial broadband seismometers, while the remaining one-third use triaxial short-period seismometers. Since 2011-2021 is a large time span a subset of stations and channels were selected for processing. The selection was based on sensor type, operational availability and stability in this time period, geographical distribution and known ambient noise characteristics. A total of 103 stations have been selected for the analysis of teleseismic events, as depicted in Figure 1.

*Figure 1: Station distribution of the **Hellenic Unified Seismic Network** (HUSN) used in this study. The orange triangles represent broadband stations where only data from Z component are utilized, while the yellow triangles represent stations that we use data from all three components.*

Given the substantial volume of data, waveforms from the Z components are exclusively employed for the majority of stations, with a focus on broadband stations. To precisely establish the onset times of S-type phases, a subset of 18 stations with three components are also examined, Figure 1. These stations are HL.ARG, HL.APE, HL.ATH, HL.GVD, HL.IACM, HL.IDI, HL.IMMV, HL.ITM, HL.KARP, HL.KLV, HL.KEK, HL.KTHA, HL.PRK, HL.SMG, HL.THERA, HL.THL, HL.VLS and HL.ZKR. These stations were chosen for their strong attributes and consistent operational performance mostly equipped with STS2-120s and Trillium-120s.", (Gkika and Havskov 2023).

THE agency reporting to the ISC

From the global earthquake solutions of the ISC under the acronym THE is the Department of Geophysics, Aristotle University of Thessaloniki. The THE agency, continuously contributes with teleseismic phases reports from Greek stations to the ISC since 2011, the time that NOA (ISC acronym ATH) ceased to report.

The THE agency, during the daily process of seismicity in Greece and surrounding areas analyze local, regional and teleseismic events. All the events that enter their system, without any magnitude restriction which are located in regions outside of their network interest, are analyzed by reading only the first clear P phases. These events can be local (≤ 1000 Km) but outside their networks interest, regional (1000-2000 Km) or teleseismic (>2000 Km). For the analyses they utilize all the stations of the HUSN (Hellenic Unified Seismic Network) plus available shared stations by neighboring countries. No location information or magnitudes measurements is given by these analyses (personal communication with C. Ventouzi and C. Papazachos, 2024).

All this information is available at THE new webpage (still under construction) at the link https://seismo.auth.gr/monthly-earthquake-bulletins/ (see Additional Phases with Greek language option activated, last checked on 18/03/2024). As can be seen there, a large number of processed events are reported, covering the period where our analyses is focusing, 2011 – 2021, Figure 2. There are 142.677 P -phases, 2457 S-phases and 731 PKP phases. The sudden increase of the number of analyzed events in the third month of 2011 coincides with the Ms 8.4 Honshu Japan earthquake on March 11, 2011.

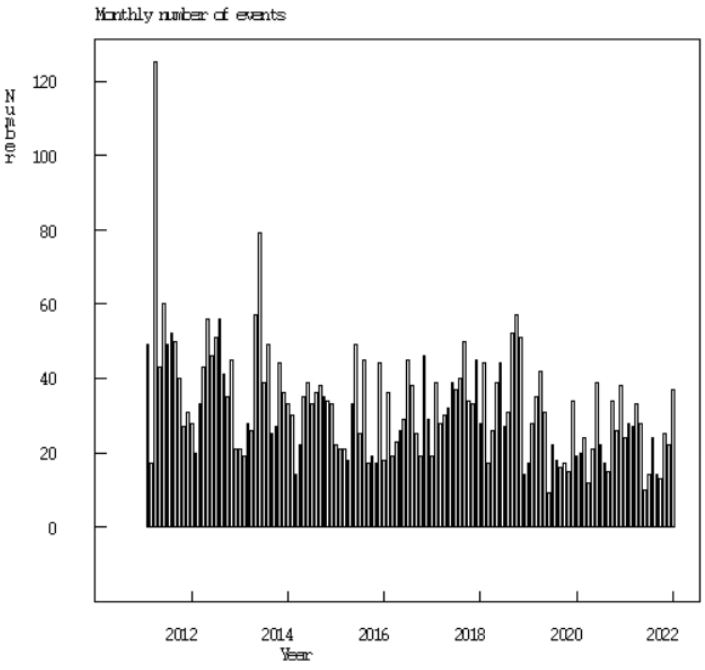

Figure 2: Monthly distribution of events (events with additional phases outside their network interest) as reported by THE agency, period 2011 – 2021.

A rough estimate is that for the period 2011-2021 THE agency has reported a total of 4383 events, Figure 3. Based on an ISC search, about 60-80 events per year are global events with magnitude mb ≥ 6.

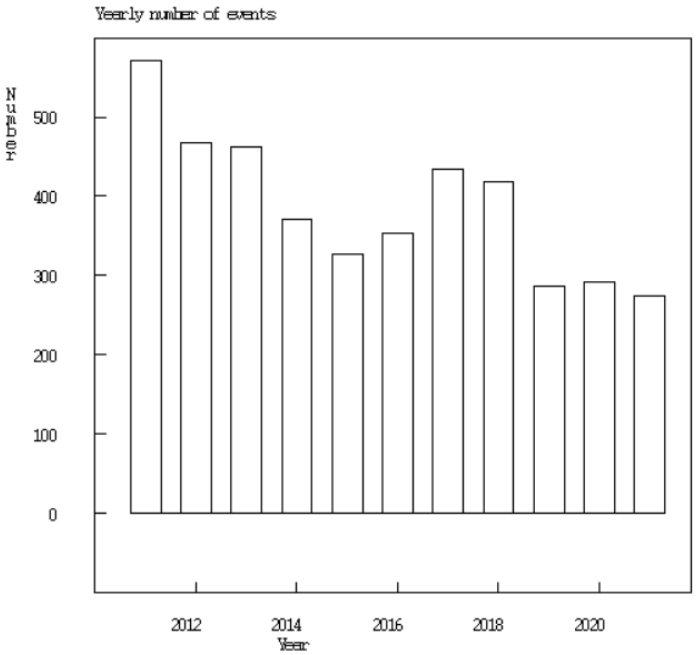

Figure 3: Yearly distribution of events (events with additional phases outside their network interest) as reported by THE agency, period 2011 – 2021.

Using solely the available information given by THE agency these events were approximately located, Figure 4. Since secondary phases or phases from global stations are absent, it was expected that these solutions would not be so accurate. Some events could not be located, some were duplicates. The final events located were in total 4191. But still, the approximate global distribution of these events indicate that they will have contributed significantly to the revised ISC solutions.

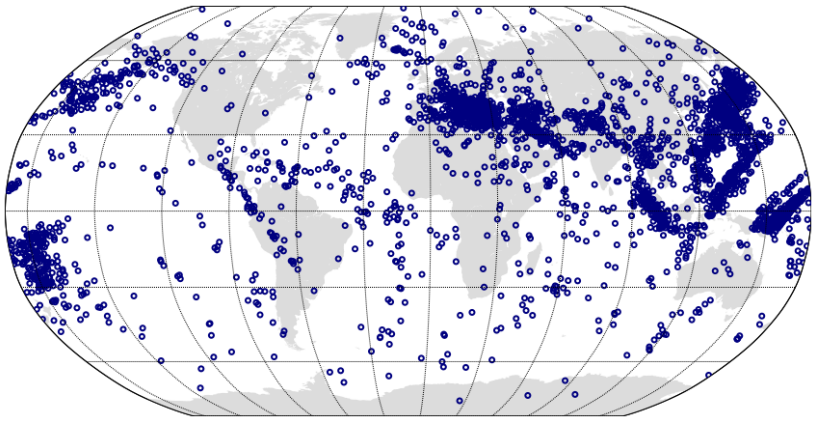

Figure 4: Events located with data by THE agency, using P phases, period 2011- 2021.

Data

"Several tests were conducted to identify events in the ISC Bulletin (International Seismological Centre, 2024) that would likely be detected by a majority of stations as global events. It turned out that selecting events with ISC mb ≥ 6.0 was a reasonable choice. The option of using all types of magnitudes from all agencies, if they are greater than or equal to 6, was dismissed due to the inclusion of unreliable magnitudes by some agencies resulting in the selection of events with magnitudes that were too small. ISC receives data from 150 different agencies and reports 39 types of magnitude, but only calculates mb and Ms (Havskov and Lieser 2021). In order to get the most reliable hypocenters, only events with hypocenters calculated by ISC were selected and only if this hypocenter was designated as the prime hypocenter by ISC. The output from the ISC search engine is hypocenter and magnitudes in ISF format (extension of IMS format)." For the period 2011-2021, there were 952 events fulfilling these criteria, see Figure 5. ISC prime solutions for large events are described with numerous phases picks and magnitude measurements for stations used around the globe, about 4000 to 5000 phases most of the time. So, phases were not included because that would make it more difficult to do the processing, see next section.

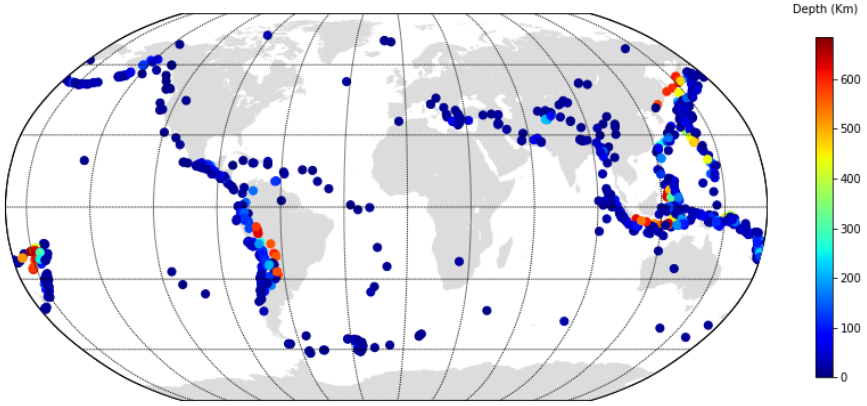

Figure 5: In the period 2011-2021, a total of 952 global events from the revised ISC catalogue were fulfilling the criteria having an ISC prime hypocenter solutions with magnitudes mb≥6.

Processing

Processing was performed using the SEISAN software (Havskov et al. 2020). Selected events waveform data for the ISC events were extracted in 2 hours sections from the Greek stations and, together with the ISC locations, inserted into a SEISAN database. This was done to secure a faster loading to avoid to read from the continuous data for the whole period. Then analysis for each teleseismic event began with the picking of P and S phases without any type characterization assuming them to be first arrivals. This was done to avoid problems with phase names in locations and thus just refers to the first phase of P or S type. The location was done with the hypocenter fixed to the ISC location in order to get accurate residuals with respect to a correct hypocenter. Using only Greek stations and no fixed solution would make it difficult to evaluate the residuals due to the uncertainty of the solutions and including all the ISC phases would make it time consuming and hard to spot the Greek stations' residual. On a second stage, well identified, later arriving phases were also picked. To help identify later arrival, theoretical phase arrivals were calculated and displayed on the screen using the IASP91 travel time tables (Kennett and Engdahl, 1991). The phase

names were based on the recommendations of the IASPEI Commission on Seismological Observation and Interpretation (Storchak et al., 2003, Storchak et al., 2011, http://www.isc.ac.uk/standards/phases/). Phase picking was done only if phases could be clearly seen, and S-type phases were picked normally only from horizontal components. Although filtering is available in SEISAN, phase picking was done with no filter, in order to avoid phase shift. Numerous different phase types were picked such as P, Pdif, pP, pPdif, PP, PKP, pPKP, S, SS, SKS. In addition, amplitudes for body wave magnitudes mb, mB and broadband surface wave magnitude MS were measured too. In the initial study of the data from 2019 (Gkika and Havskov 2023) it was shown that the surface magnitudes reported by NOA MS and Ms were very similar and thus it was decided to measure only broadband MS for the rest of the catalogue. This also avoids the problem of formally having to pick amplitudes for Ms in the period range 18-22 s. A more detailed description of the picking and location process that was followed is given in the pilot study, (Gkika and Havskov 2023).

Often, in cases where the initial phases, such as P or Pdif, were undetectable, picking the later arriving PP phases, characterized by higher amplitudes, was a solution to the location analysis. At larger teleseismic distances where PKPdf were detected as first P arrival (for example at 15000 kilometers), a few PP phases (if present) could help to constrain the solution. Depth phases such as pP or pPKPdf, usually were clear for deeper events while it was a challenge to distinguish them for surface events. They could not be discriminated at all for shallow events, such as those at around 10 kilometers depth. In general, deep events had distinct and clear phases arrivals compared to near surface events so deep events usually contributed with more phases than shallow events.

Events not processed

In total 137 events were not processed from the 2011 – 2021 data set (Table 1). Among them 18 were local and one regional event, these were excluded from the analyses because they had already been processed by NOA, see Figure 6. The majority of the not processed events were shallow events at intermediate to large teleseismic distances. These events had very unclear low frequency P and not many other clear phases, see example Gkika and Havskov (2023). The other problematic events were events where their waveforms were a mixture of two events. This was either aftershocks recorded within the records of the main event or two events occurring at the same time at different locations. Examples in Appendix II. Some low signal/noise cases could not be analyzed because we did not use filter. However, it is revealing that even magnitude mb 6 events cannot always be analyzed and certainly not located by HUSN.

Table 1:Events not processed due to various causes.

Events not processed	
Local & Regional	*19*
Two events at same origin time and different locations	*3*
Aftershocks mixed with main events	*43*

Low frequency event, low signal/noise ratio	*72*

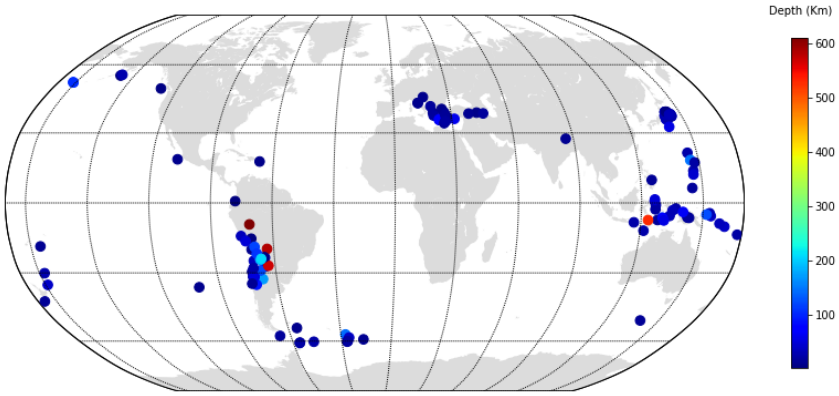

Figure 6: Events not processed with magnitude mb≥6 (ISC), a total of 137.

Analyzed events

The final number of events analyzed were 815, which represents the 87.3% of the originally selected events with mb≥6, for the period 2011-2021. A 59% of the originally selected events had already been reported to the ISC by THE agency, but still a 29% of the teleseismic events are missing. These are included in our current work and are fully analyzed.

A summary of the number of phases and amplitudes obtained in this study is presented in Table 2. In contrast is shown additionally what is already reported by THE agency to the ISC in order to get an idea of what NOA actually has contributed. The identification of phases, is clearly reflected in the numbers and the different types of them.

Table 2: A comparison of number and types of phases obtained by the two reporting Greek agencies for our test data set. Phase types given by NOA are derived from our analysis while phases types from THE agency are not the originally reported but the ones identified by ISC.

Phase types	***Count***	
	NOA	***THE***
P	*39036*	*23554*
pP	*6350*	*25*
Pdif	*653*	*2968*
pPdif	*338*	*0*
PP	*15214*	*789*
PKPdf	*3905*	*6809*
pPKPdf	*3438*	*58*
PKPab	*92*	*676*
PKPbc	*123*	*906*
PKPpre	*0*	*666*
PKiKP	*0*	*986*
PKKPdf	*0*	*12*
PKKPbc	*0*	*22*
pPKPbc	*0*	*7*
sP	*0*	*1*
S	*6024*	*229*
SKP	*7*	*0*
SKPbc	*0*	*50*
SKSac	*0*	*187*
SKKSac	*0*	*64*
SS	*472*	*0*
Total	***75.652***	***38.009***
Magnitudes	***NOA***	***THE***
IVMs_BB	*29043*	*0*
IVmB_BB	*21919*	*0*
IAmb	*21570*	*0*
IAMs_20	*2851*	*0*
Total	***75.383***	***0***

Table 2, shows that our study has obtained quite a lot more phases than the phases were sent to the ISC from THE agency. THE did not read many S-type phases (probably since this is more time consuming) so nearly all phases are of P-type. The phases shown from THE are the phase names identified by ISC, so phases like e.g. Pdif and PKPdf were reported to ISC as first arrivals P and then later re-identified. If we

sum the P type phases for THE, we have nearly as many as our P phases indicating that for nearly all events, a P-phase were read. This can be explained because THE agency uses more stations (>150), we used only the broadband stations of HUSN (103). The current analyses was set up to measure magnitudes too. A more detailed comparison could be done by using the same stations for both datasets; to check phases reports per station but this is out of the scope of this work.

Most agencies with agency names e.g. THE, NEIC, GFZ, MOS as reported to ISC (2024b) only read first arrival P for Greek stations, so our study has clearly enhanced the teleseismic data base for HUSN by adding a significant amount of secondary phases. In addition, many amplitudes for different magnitudes have been added so we can easily conclude that in total, much more information is now available for teleseismic events from HUSN.

For the 815 events, ISC has reported **8989** readings of mB and **11274** of MS. So, it is clear that the NOA data has significantly contributed to an increase in the number of broadband magnitude reports by a factor of 2-3 for the time period 2011-2021.

In addition, considering the secondary phases a comparison of them with respect to what has already been reported to the ISC for the analyzed 815 events, is presented Table 3. These are expressed with the relative number of phases picked, that is the number of phases in comparison to the number of P-phases.

Table 3: Number of some phases in percent of number of P-phases for different data sets. ISC 815 is the ISC data for the 815 large events, ISC all are all readings used by the ISC in the relevant time period (Data provided by Kathrin Lieser at ISC) and NOA is the data picked in this study.

	PKPdf	S	Pdif	PP	SS	pP	mb
ISC 815 mb>=6	18	15	8	5	3	2	43
ISC all magnitudes, 1970-2021	8	5	1	2	0.7	2	
ISC all magnitudes, 2011-2021	7	4	1	1	0.6	1	
NOA 815 mb>=6	9	15	0.2	3	0.1	16	56

It should be noted that the phase names used by ISC is not the names submitted but the names identified by the ISC program so e.g. PKPdf is most likely reported as P. This is also the case for Pdif. In the NOA data set it is the phases read.

It seen that in our study, only pP and amplitude for mb, MS and mB has been reported relatively more frequently than in the ISC data set. For the S-type phases, this is probably because we only used 18 out of 103 stations with 3 components to read S-type phases. If we had used all, we would probably have read 4 to 5 times more.

Location Comparison

The comparison of teleseismic locations by NOA using only phases from selected Greek stations and the prime solutions of the ISC are presented in Figure 7. The purpose of this comparison is to evaluate how well the Greek network can locate teleseismic events although the global network of course will do a much better job. The majority of the large teleseismic events are mainly concentrated along converging plate boundaries. It can be seen that the major Pacific plate and its adjacent microplates contribute the most. "Earthquake source parameters calculation was done with the **hypocenter** program (part of SEISAN) that locates teleseismic events. It is a modified version of HYPOCENTER (Lienert et al., 1986; Lienert, 1991; Lienert and Havskov, 1995). It should be noted that SEISAN uses IASP91 (Kennett and Engdahl, 1991) earth model while ISC uses Ak135 (Kennett et al., 1995) so there will be small differences in the travel times calculated by the 2 models". Additional differences can be due to the fact ISC uses a different location algorithm ISCloc (Bondar and Storchak, 2011) and of course a global station network where all events used here were located with more than 1000 stations.

For the total of the dataset covering the period 2011 - 2021 results are quite good. Even the few events with the largest deviations are located with satisfactory accuracy by the Greek stations, despite the large teleseismic distances. This confirms the outcome of the pilot study for data form 2019, (Gkika and Havskov 2023).

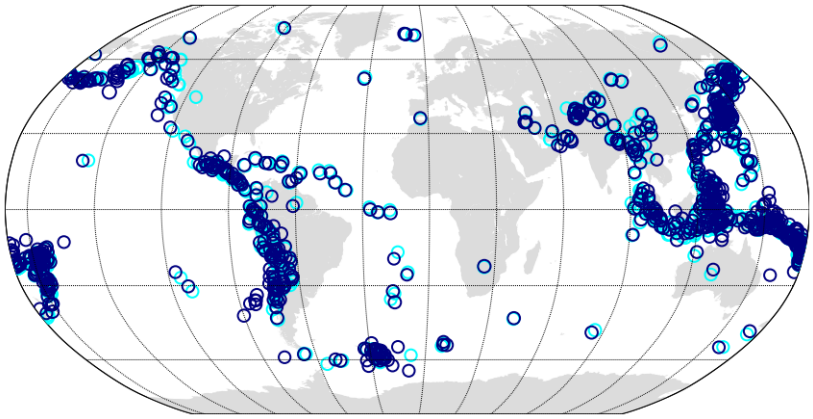

Figure 7: Comparison of teleseismic locations by NOA as derived solely from phases from selected Greek stations (dark blue) and the prime solutions of the ISC (light blue).

Several location comparisons were done in order to investigate probable failures of the picking process and evaluate the quality of the analysis. In a first stage, by comparing the locations of the NOA data with fixed hypocenter and unfixed origin time with the original ISC solutions, about 12 events were detected deviating in origin time and were reexamined. These were mainly large distance teleseismic events and the problem was that our location program assigned a wrong name to the P phase read. So, in these cases the correct PKP type phases were assigned manually. In cases where waveform recordings have a mixture of events at this stage it is useful to detect problems (e.g. analyzing the wrong event) as it is expected to

exhibit extreme origin time residuals (see Appendix II). The average difference in origin time using our data and the origin time reported by ISC was 0.6+/-1.0 s. This indicates that our readings are reasonably correct and the average difference is probably due to using different travel time models.

Comparing the NOA data solutions using unfixed hypocenter to the ISC solutions, can be seen higher values in origin time and depth on both average and standard deviation. This is due to the fact that is not possible to achieve a good location in some events. When locating without fixing the hypocenter to ISC, in some cases a bad location was obtained due to our program was making a bad start location when using only the Greek stations. So, for all events, the ISC epicenter was used as start location, see Table 4. In epicentral terms values are then minimized. But is evident that the most significant deviations is seen in hypocentral parameters in terms of depth, particularly for the deepest events.

Table 4: Comparing the average hypocentral parameters between ISC and NOA locations using unfixed hypocenters and using start location. Coordinate differences are expressed in degrees and Depth in Km.

	Origin time	RMS	Lat	Lon	Depth
Average diff	-3.4	0.3	-0.253	0.026	-42.9
Standard dev	20.5	0.3	2.161	2.729	150.6

Our epicenters are close to the ISC epicenters but the depth and consequently the origin time have large differences.

Table 5: Comparing the average hypocentral parameters between ISC and NOA locations using unfixed epicenters and using start location and fixed Depth. Coordinate differences are expressed in degrees and Depth in Km.

	Origin time	RMS	Lat	Lon	Depth
Average diff	1.1	0.7	-0.227	0.105	0.0
Standard dev	12.9	0.4	2.056	2.711	0.0

Fixing the depth improves the locations and origin times as seen by comparing to Table 4. The importance of picking depth type phases is investigated by using only events with pP phases (Table 6) It is seen that using pP phases further improves the locations. It should be mentioned that events with pP phases usually are deep with clear phases which again will improve the quality of the locations.

Table 6: Comparing the average hypocentral parameters between ISC and NOA locations, only for events with depth phases pP, using unfixed hypocenter. Coordinate differences are expressed in degrees and Depth in Km.

	Origin time	RMS	Lat	Lon	Depth
Average diff	0.6	0.8	-0.102	0.156	-2.3
Standard dev	4.9	0.3	1.237	1.493	5.1

In the current analyses, almost half of the total events, 383, have depth type phases such as pP, pPdif or pPKP reassuring a good location quality.

Despite that, locating events solely by Greek stations at large teleseismic distances due to insufficient azimuthal coverage has disadvantages from the beginning. In general, reasonably well-constrained teleseismic solutions can be achieved when there are at least 10 usable first arrivals from teleseismic stations and when the azimuthal coverage of these stations is greater than 180°, (Engdahl, et al 1998). In terms of depth better results would be accomplished only with the use of additional global stations.

Although well constrained global location cannot be expected for the Greek network, locating teleseismic events helps to check the quality of the observations.

To investigate further the potential impact of introducing NOA solutions to the ISC prime solutions, six events were selected which had no reports of phases from THE agency. The prime solutions with ISC phases were relocated with SEISAN to investigate the difference in solutions to ISC using SEISAN and the IASP model. Subsequently, for each event, the additional phases from HUSN stations were inserted and the events relocated. Then the two SEISAN locations were compared and the difference between the two solutions will only be due to entering the HUSN data and not due to using different program and travel time models. See Table 7.

Table 7: Comparing locations of 6 test events which did not include data from THE at the ISC. Abbreviations: 1st: ISC solution, sei: the relocation of ISC solution in SEISAN and NOA: the relocation of the event with the ISC phases included in the original solution plus the phases by NOA. Abbreviations refers as Date and Time of origin time of the teleseismic event, Lat: Latitude, Lon: Longitude, Depth in km, rms: root mean square of travel time residuals (s), mb: body wave magnitude from ISC, ISC phases: number of phases used in the ISC solution, NOA phases: number of phases used from HUSN selected stations in the solution, ISC mb: number of amplitude readings for mb from ISC, NOA mb: number of amplitude readings for mb from HUSN stations.

No	Date	Time	Lat	Lon	Depth	rms	mb	ISC phases	NOA phases
1st ISC	20140412	201438.6	-11.258	162.139	15	1.7	6.9	3306	206
sei	20140412	201438.6	-11.176	162.089	12	1.6			
noa	20140412	201438.6	-11.180	162.093	12	1.5	6.8		
2nd ISC	20140614	111103.3	-10.113	91.038	23	1.9	6.2	2616	90
sei	20140614	111103.3	-10.023	90.990	22	1.7	-		
noa	20140614	111103.5	-10.027	90.978	24	1.7	-		
3rd ISC	20140623	205309.1	51.703	178.643	102	2.2	7.1	3818	115
sei	20140623	205309.3	51.777	178.824	101	1.5			
noa	20140623	205309.6	51.770	178.834	104	1.6	7.0		
4th ISC	20140624	031538.9	52.009	176.782	23	1.8	6.0	2582	69
sei	20140624	031539.0	52.108	176.867	25	1.5	-		
noa	20140624	031539.0	52.106	176.864	25	1.5	-		
5th ISC	20140925	175117.9	61.986	-151.916	107	1.7	6.0	2906	70
sei	20140925	175118.8	62.028	-151.841	111	1.3			
noa	20140925	175118.8	62.031	-151.844	112	1.4			
6th ISC	20141210	210340.3	25.530	122.463	267	1.6	6.0	2545	92
sei	20141210	210340.7	25.588	122.444	267	1.1			
noa	20141210	210340.7	25.591	122.437	267	1.1	6.0		
AVERAGE DIFFERENCES									
sei-ISC		0.27	0,07	0,04	0.17	-0,37			
noa-ISC		0,35	0,07	0,00	0.17	-0,35			

Results of adding NOA data do not differ significantly from the original prime ISC solutions. This is not surprising, as a network with a small geographic extent cannot dramatically affect the hypocentral parameters of a teleseismic event, particularly for events recorded with more than 2500 stations

However, the small change in location indicate that the Greek observations are reasonably correct. Still is noticeable considering that 150 agencies report to the ISC and contribute to the final solutions, what a single network can report.

Magnitudes

"One purpose of this study is to compare magnitudes calculated by NOA and the prime magnitudes calculated by ISC. ISC only calculates body wave magnitude mb and surface wave magnitude Ms, Di Giacomo and Storchak (2016). Both magnitudes are based mainly on the relatively narrow WWSSN standard seismograph response. However, in recent years, these magnitudes have also been calculated using a wider response, the so-called broadband body and surface wave magnitudes, respectively mB and MS. These magnitudes will also be calculated in order to investigate the differences with mb and Ms. For detailed definitions, see the latest IASPEI standards, by Bormann and Dewey, 2014:

Magnitude mb is a derivative of mB definition by Gutenberg (1945 a, b, 1956) and is calculated from the maximum amplitude in the P-wave train. It is defined as:

$mb = \log(A/T) + Q(\Delta, h)$ (1)

where A is the maximum amplitude in nm or μm (depending on which Q-function is used), T the period and Q the attenuation function as a function of epicentral distance Δ and hypocentral depth h. It is recommended by IASPEI to use the original attenuation functions for P waves (Gutenberg and Richter 1956), which are been used nowadays by the ISC and USGS. This relation has also been used in our study.

The magnitude relation for broadband mB is in agreement with the original definition by Gutenberg and Richter (1956), which used a wider response than used for mb. It is defined as:

$mB = \log (Vmax/2\pi) + Q(\Delta, h) - 3.0$ (2)

where Vmax is maximum ground velocity in nm/s recorded on a broad band sensor proportional to velocity and Q is the correction function mentioned above. Body wave magnitudes mb and mB have no depth restrictions. Amplitude measurements are restricted only in the period range. The mb is calculated in the period range of 0.2-3 sec and mB in the period range of 0.2-30 sec. As a result of the short period range on measurements of mb, it saturates around magnitude 7 while mB saturates at around magnitude 8. Both magnitudes are calculated in the distances 20°–100°".

Surface wave magnitude was introduced by Gutenberg (1945), is based on the measurements of surface waves amplitudes using the vertical component and generated by shallow earthquakes < 60 Km, defined by the Moskow – Prague formula:

$Ms = \log (A/T)max + 1.66 * \log\Delta + 3.3$ (3)

where A is amplitude in μm, T period in sec, and Δ distance in degrees from the epicenter (Karnic et al. 1962, Vanek et al. 1962, IASPEI 2013). Ms is measured in the distance range 20° -160°.

The Ms magnitude, although depth limited, has the advantage that it can be used for magnitude calculations of earthquakes at a larger distance range than mb."

Among all magnitudes, Ms is the most frequently reported from the early instrumental seismology, particularly in the northern hemisphere were the seismic networks originated and became denser through time (Di Giacomo and Storchak, 2022)." Since the early 60s and after the introduction of WWSSN (World-Wide Standardized Seismographic Network), in most agencies, Ms calculations refers to measurements of surface wave amplitudes applied in a narrow period range between 18 – 22 sec and teleseismic distances 20° – 160°, (Oliver and Murphy, 1971; Peterson and Hutt, 2014, Di Giacomo 2022).

Broadband magnitude MS in contrast with Ms, is used in wider distance ranges between 2◦ to 160◦ and a wider period ranges of 3 to 60 s. The larger period means that, for large events, the magnitude is less affected by the local structure. The smaller period and the smaller distance mean that mB can be used for local and regional events. Broadband mB could have a much wider use and applicability and is particularly valuable for large regional events, however it is not much reported to the ISC yet.

All these magnitude types mb, mB, MS have been calculated for the available dataset with respect to their restrictions by definition and following the IASPEI standards on amplitude and period.

Magnitude residuals – station check

An extensive search has already been conducted considering the stations used by HUSN mainly in order to detect probable technical problems (Gkika and Havskov 2023). By comparing ground motion data with a reference station KLV that has zero magnitude residuals and analyzing noise spectrums for gain or installation issues, many stations were checked, and no problems were detected. This process was initially done to ensure the accuracy of magnitude readings for selected stations in the present work.

In order to check further the magnitudes, average station magnitude residuals are recalculated for all stations using the whole dataset (see Appendix I). The residuals calculated as the difference between the average event magnitude and the station magnitude. The most deviating stations (average residual ≥ 0.25) are presented in Table 8. The deviating magnitudes for the dataset of 2011-2021 are shown, as detected per station in at least one magnitude.

Table 8: Stations of HUSN with average magnitude residuals higher than 0.25 checked for magnitudes mB, mb, and MS. Abbreviations: STAT station name, N number of magnitude measurement counts, AV average magnitude residuals, SD standard deviation of the magnitude residuals. Body wave magnitudes mb short period, mB broadband and broadband surface wave magnitude MS.

AVERAGE MAGNITUDE RESIDUALS DEVIATING ≥0.25									
mb				*mB*			*MS*		
STAT	*N*	*AV*	*SD*	*N*	*AV*	*SD*	*N*	*AV*	*SD*
ARG	*305*	*0,25*	*0,23*	*314*	*0,17*	*0,17*	*187*	*-0,26*	*0,15*
KARP	*305*	*0,25*	*0,29*	*304*	*0,2*	*0,2*	*411*	*-0,02*	*0,16*
KARY	*178*	***0,19***	***0,47***	***177***	***0,24***	***0,43***	***216***	***0,25***	***0,41***
THL	*316*	*-0,28*	*0,28*	*325*	*-0,19*	*0,14*	*488*	*0,03*	*0,11*
IACM	*197*	*0,43*	*0,26*	*184*	*0,22*	*0,23*	*407*	*-0,11*	*0,17*
CMBO	*3*	*0,28*	*0,2*	*3*	*0,12*	*0,28*	*6*	*0,06*	*0,29*
MDRA	*33*	***-0,29***	*0,23*	*31*	***-0,22***	*0,18*	*14*	*-0,03*	*0,08*

Most of the stations have already been checked in detail and no technical or other problems were detected apart from some high noise levels. The stations KARP, ARG, THL, IACM were checked for soil amplification as given by Ktenidou et al. (2026) and the residuals do not seem to be related.

However, KARY is a station that had not been checked initially. Only when using a larger dataset, the station shows slightly positive high average residuals across all magnitudes and extreme standard deviations. High standard deviation usually points an instrument malfunction, a problem in the metadata for a specific time period or a deviation in magnitude readings for specific events (usually wrong readings). Plotting station KARY residuals as a function of time, it was obvious that there was a response error in the first time period, see, Figure 8.

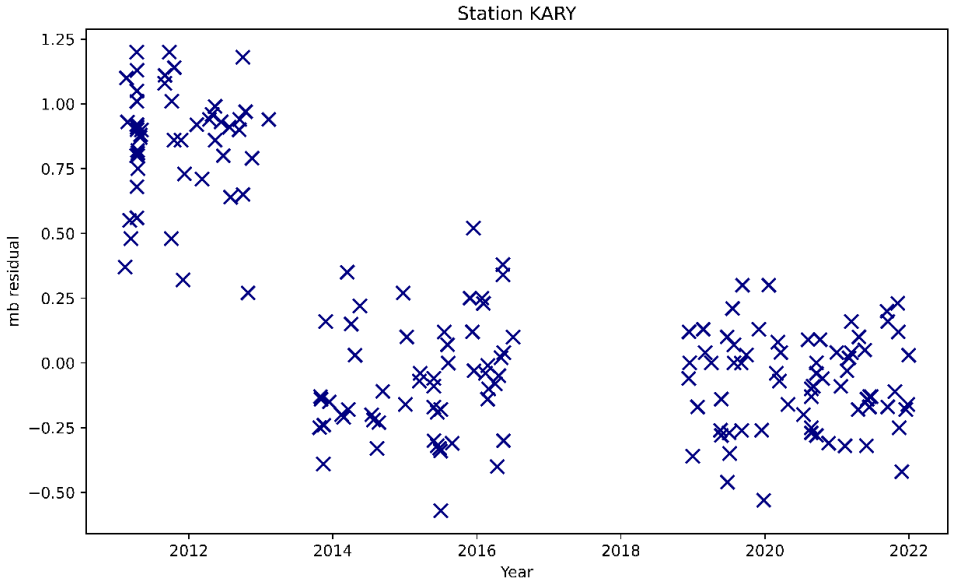

Figure 8: Distribution of magnitude mb residuals per year for KARY station, period 2011 - 2021.

So, this analysis allowed us to identify and resolve the problem, thereby correcting the station's response and reading again the magnitudes for the problematic time period, see Figure 9, the problem was fixed.

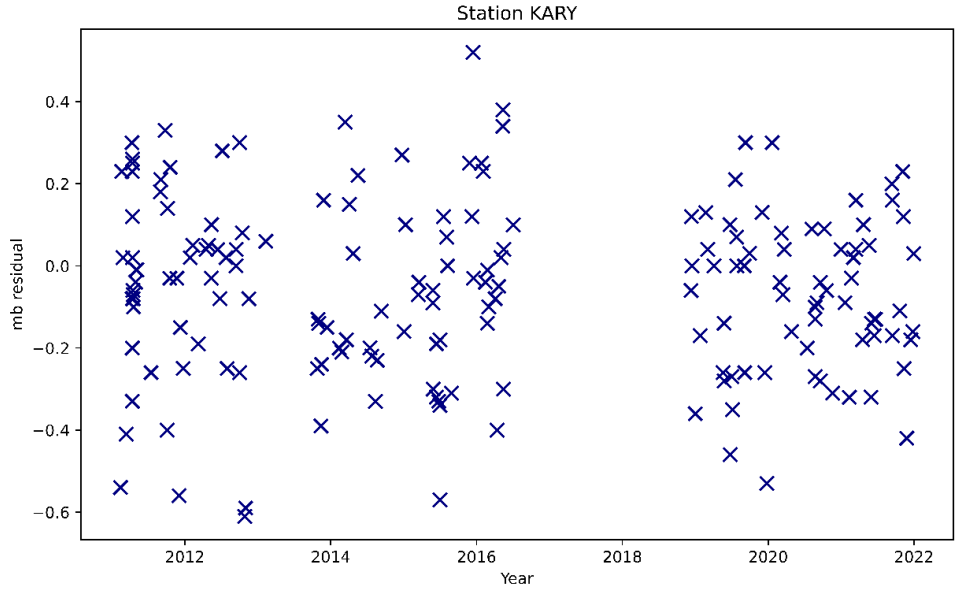

Figure 9: Distribution of magnitude mb residuals per year for KARY station, period 2011 – 2021 using the corrected response file.

Since the KARY station is also used for ML for local earthquakes, the ML residuals for the period with wrong response file was checked and it also showed positive residuals, see Appendix III.

Magnitudes Comparisons

For the analyzed teleseismic events of the period 2011 - 2021, comparisons have been made between the different calculated magnitudes by NOA (mb, MB, MS) and the magnitudes reported by ISC (mb, Ms). All magnitude comparisons were made fixed to the ISC Prime **Hypocentral** solutions. They are presented in the following paragraphs with their derived empirical relations which were calculated with maximum likelihood, a mathematical method to approach best fit. These are the final results because prior comparisons were used to detect the most outlying events. These events were reexamined in order to detect any measurement problem affecting the magnitude due to a station problem (e.g. KARY) or wrong magnitude readings made at events with low signal to noise ratio

Compare NOA mB and mb

Comparison of NOA calculated magnitudes for broadband mB and short period mb, is shown in Figure 10.

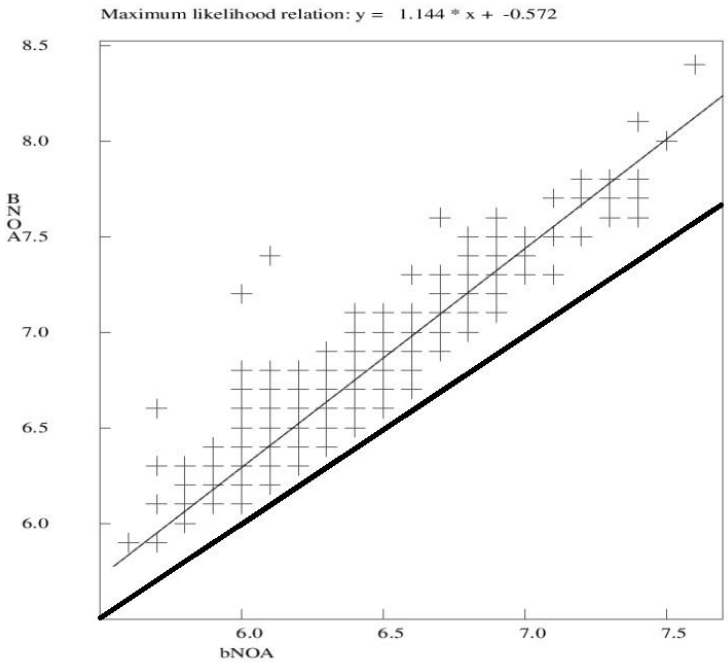

Figure 10: Comparison between body wave magnitudes short period mb and broadband mB by NOA, fixed to the ISC prime hypocenter solutions. Dataset used refers to the period of 2011-2021, for events of ISC revised catalogue with magnitude Mb≥6. After reviewing the outlying events and magnitude readings. The 1:1 relation is also shown, blue line.

Average values of magnitudes mb, mB are 6.37 and 6.71 respectively and the correlation is strong, 0.92. The difference in the two magnitudes increases with magnitude indicating that the mb scale saturates for

all magnitudes in our magnitude range. When mB is 6 standard mb is 5.7 which seems a bit large. Ideally one should have had more data with smaller magnitude to see exactly at which magnitude the two magnitudes are similar.

The deviation on the mb, mB comparison by NOA is indicating a probable magnitude saturation on mb measurements and/or systematic differences in mb and mB.

The maximum likelihood best fit, is:

mB(NOA) = 1.144* mb(NOA) - 0.572 (4)

For NOA catalogue, mB magnitude shows higher average value in comparison with all the other magnitude types MS(6.49), mb(6.37)).,

Average broadband mB by NOA is 0.34 higher than mb by ISC. This is in agreement with the observation that magnitude mB on average is 0.7 units larger than mb, (Kanamori and Ross 2019).

Compare mb NOA to mb ISC

Comparison of mb between NOA and ISC, is shown in Figure 11.

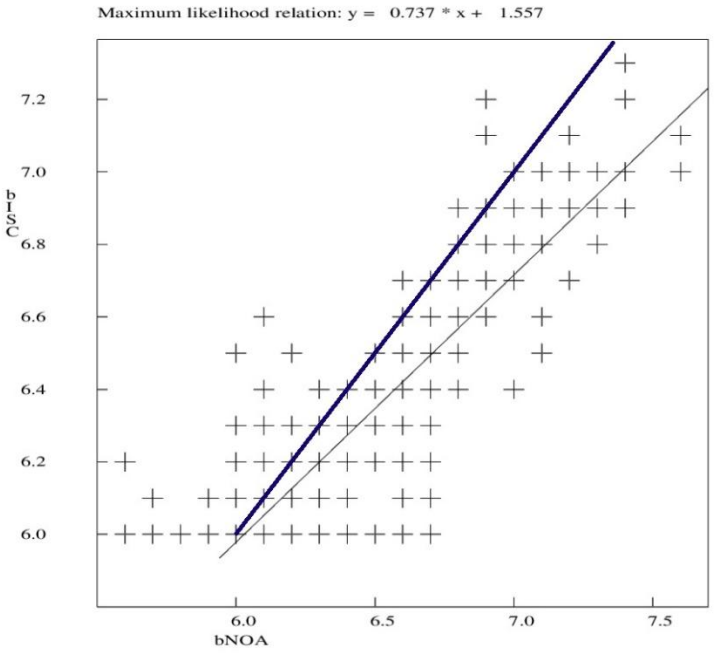

Figure 11: Comparisons of body wave magnitude mb, between ISC and NOA. The dataset used refers to the period of 2011-2021, for events of ISC revised catalogue with magnitudes mb≥6. The 1:1 relation is also shown, blue line.

The figure shows quite a lot of scatter, however for mb deviations of half a magnitude unit between different stations and network is quite common. The majority of the magnitude reports per event were derived as the average of many readings reassuring a magnitude stability and the reason for the scatter is

probably not related to errors in our magnitude determination and the average magnitudes for the two data set are also very similar with mbNOA 6.37 and mbISC 6.25. However, the differences in average indicate that NOA give a higher magnitude than ISC and from the figure this is particularly clear for larger magnitudes. The best fit line with Maximum likelihood is:

mb(ISC) = 0.737 * mb(NOA) + 1.557 (5)

Compare MS NOA to Ms ISC

Comparison of standard Ms versus broadband MS between ISC and NOA/GI respectively is shown at **Error! Reference source not found.** Figure 12 . MS by NOA was decided to be calculated for the whole dataset 2011-2021 because with the comparisons using a smaller dataset for 2019, it was found that Ms NOA and MS NOA were similar, (Gkika and Havskov 2023). The Relation is close to 1:1 and there seems to be no indication of magnitude saturation maybe because there are not many events of high magnitude in the studied period. In addition, ISC data shows that many Ms observations used by ISC also have periods outside the range 18-22 s (Havskov and Lieser 2021). Scattering is notable but magnitude readings are correct and no error were found by an extensive magnitude check on the most deviating events.

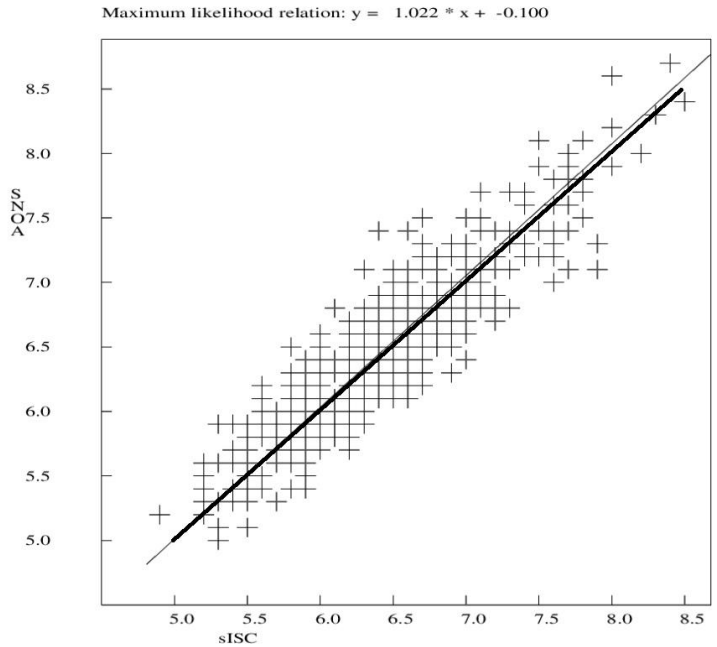

Figure 12: Comparison of surface waves magnitude Ms ISC and MSNOA. The dataset used refers to the period of 2011-2021, for events of ISC revised catalogue with magnitudes mb≥6.

The average of the two datasets for ISC and NOA are 6.44 and 6.49 respectively so on average NOA MS seems to be correct. The Maximum likelihood relation is:

MS(NOA) = 1.022 * Ms (ISC) - 0.1 (6)

Regional/Global dependency of MS and mb NOA magnitudes

It is well known that global magnitude residuals derived from a single station or a small seismic network exhibit regional variations due to differences in wave propagation paths to various regions (Selby et al., 2003). During the early stages of our analysis, we observed indications of regional variability in surface-wave magnitudes. This variability was initially identified through systematic differences between NOA MS and ISC Ms estimates for certain teleseismic events at relatively short epicentral distances.

To further investigate a potential regional or global dependency, event-based magnitude residuals were calculated as the difference between MS NOA and MsISC (Figure 13). When global magnitudes are used, station residuals are averaged over the contributing stations; similarly, averages derived from the local network represent residuals over a broader area. Consequently, these averaged residuals are expected to primarily reflect propagation path effects.

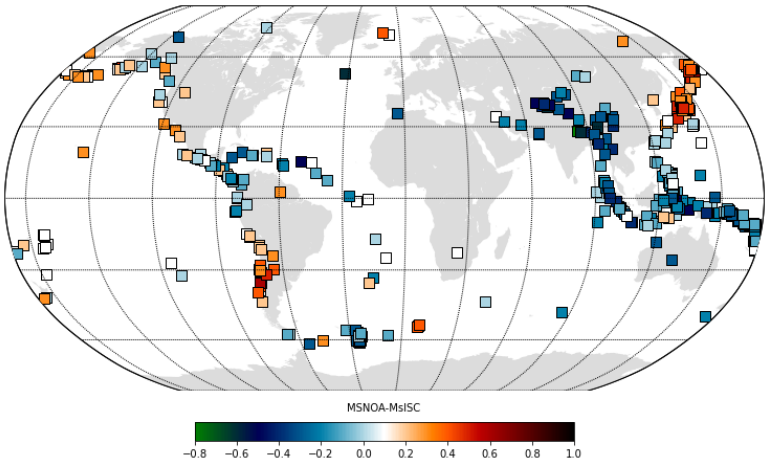

Figure 13: Global map of surface magnitude residuals per event, as derived from MSNOA – MsISC, covering the period of 2011 - 2021.

From Figure 13, it is clearly seen that we also observe a systematic variation in magnitude residuals for events with different travel paths from Greece. The distribution of the selected large events in our catalogue concentrates at the boundaries of major tectonic plates and their adjacent microplates. The positive residual distribution coincides with events along the northern and some western parts of the Pacific Plate (along the Americas and extending up to Japan). The negative residuals are clearly detected along the boundaries of the Indian Plate with the Eurasian Plate, and continuing southward with the Australian Plate, and also along the boundary between the Australian Plate and the Pacific Plate to the

south. This distribution of the residuals shows a global variation clearly controlled by the largescale tectonics.

Global patterns of events Ms residuals from a single region have been noticed by other studies (Selby et al. 2003) as seen in Figure 14**Error! Reference source not found.**. Among the top and bottom figures the residuals patterns for the same events are shown but for two different stations in Spain and Norway, resperctively. The residuals are calculated using average event Ms from a set of CTBTO stations, where a uniform way of calcualting Ms is employed and thus supposedly more stable than from a mix of station from the global network. However, since only a single station is used for calculating residuals, they might be biased by the station residual.

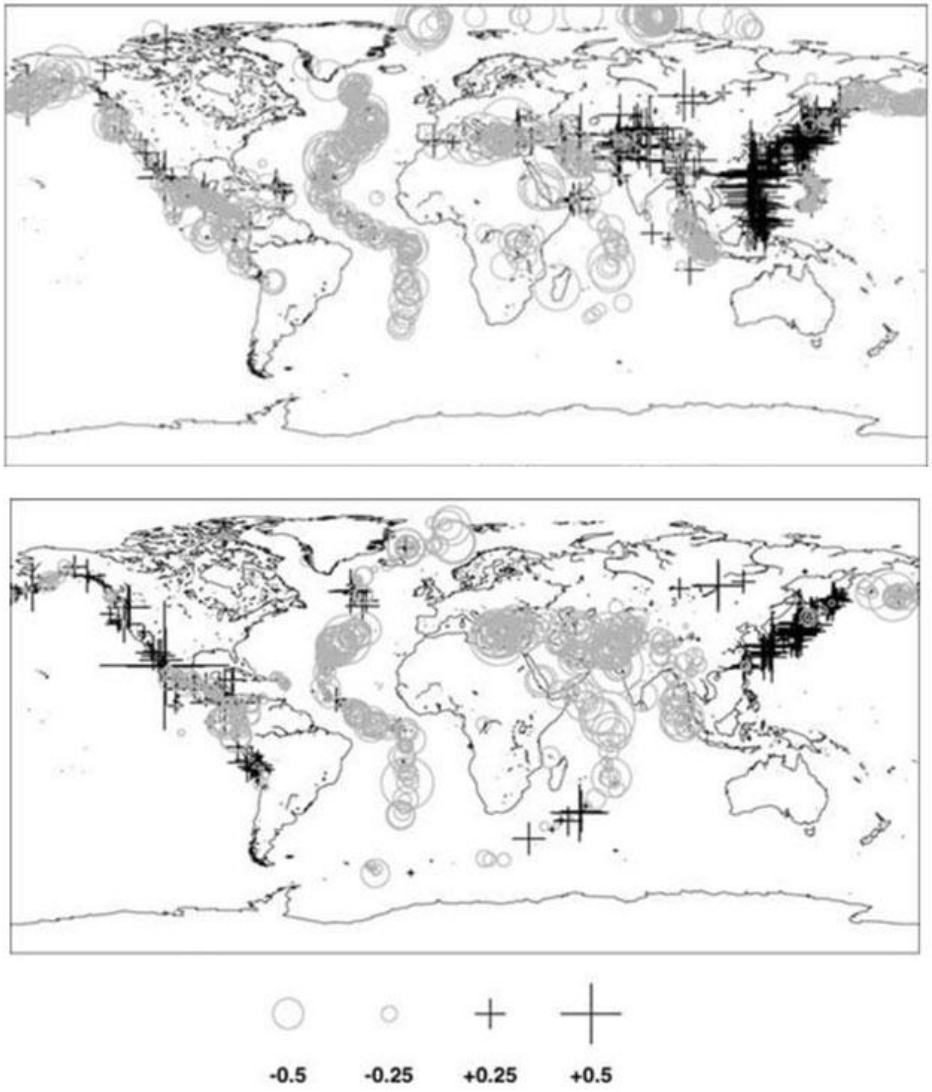

Figure 4: Global residual maps as presented by Selby et al. 2003. Top: Observed Ms residuals at station NOA Norway. Bottom: Observed events residuals at station ESDC (Spain). Negative grey circle residuals indicate that Ms observed is below the mean of the event Ms.

The two stations show similarity in the distribution of the residuals despite using two different stations. The residuals also show similarities with our results, which is not surprising since all stations are in Europe.

Magnitude residuals of magnitude mb were also calculated as the difference between mbNOA and mb ISC, Figure 13. The mb residuals show no systematic global dependency and the scattering of residuals is probably related to smaller scale tectonics. A direct comparison among body wave and surface waves events residuals cannot be done since they travel through different paths.

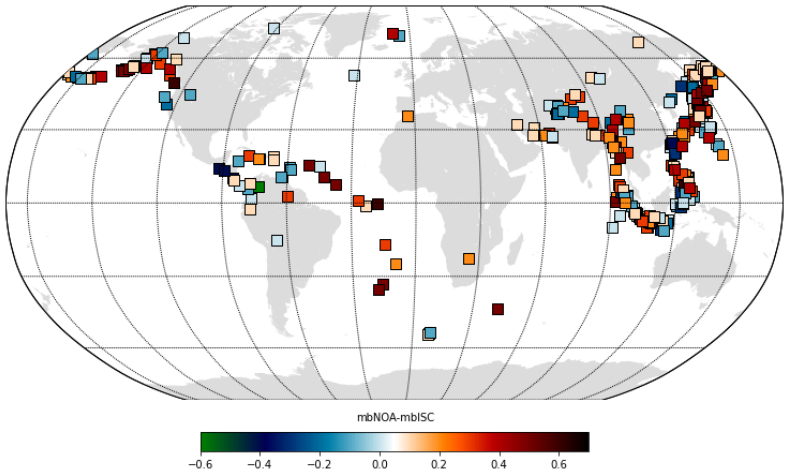

Figure 13: Global map of surface magnitude residuals per event, as derived from mbNOA – mbISC, covering the period of 2011 - 2021.

Conclusions

Global events in the time period 2011-2021 with magnitudes mb ≥ 6 for 103 stations of the NOA network have been analyzed in terms of phase and amplitude readings and location and magnitudes were calculated. This data has not been analyzed previously by NOA. Instrumental parameters were checked and found ok. The results, shows that the NOA network can make accurate magnitudes and location of global events, and it can be concluded that the network is well calibrated due to the accuracy of the magnitudes. Surface wave event residuals show a clear regional pattern also observed in other studies while global event mb residuals do not show a systematic pattern.

In general, reading of phase arrival times and amplitudes for global events have been declining in recent years and this data set makes a significant contribution to the ISC data base, particularly in terms of secondary phases and amplitudes for broad band magnitudes. NOA will now continue to process teleseismic events and hopefully this work will encourage others to do likewise.

Acknowledgments

This work is founded as Int. Scholarship by the National Observatory of Athens. Special thanks to K. Lieser helping us with ISC data, C. Evangelidis help in stations check to detect stations response problem, C. Ventouzi and C. Papazachos explaining THE data, O-J Ktenidou with C. Evangelidis help in writing the scholarship proposal. Special thanks to the agencies/analysts contributing to global events solutions.

References

Bondar, I. and D. Storchak (2011). Improved location procedures at the International Seismological Centre, Geophys. J. Int., 186 (3), 1220–1244, https://doi.org/10.1111/j.1365-246X.2011.05107.

Bormann P. and Dewey J.W. (2014). The new IASPEI standards for determining magnitudes from digital data and their relation to classical magnitudes. In: Bormann. P. (Ed.). New Manual of Seismological Observatory Practice 2 (NMSOP-2). Potsdam. Deutsches GeoForschungsZentrum GFZ, pp. 1-44. https://doi.org/10.2312/GFZ.NMSOP-2_IS_3.3.

Bormann, P. (Ed.), (2012). New Manual of Seismological Observatory Practice (NMSOP-2), IASPEI, GFZ German Research Centre for Geosciences, Potsdam; http://nmsop.gfz-potsdam.de; DOI:10.2312/GFZ.NMSOP-2 .

Di Giacomo, D., and D. A. Storchak (2016). A scheme to set preferred magnitudes in the ISC Bulletin, J. Seismol. 20, 555–567, doi:10.1007/s10950-015-9543-7.

Di Giacomo D. (2022). Bring Back Systematic Broadband Surface-Wave Magnitude Practice. Seismological Research Letters, Vol 93, no 5, pp. 2413–2417. doi: 10.1785/ 0220220094.

Engdahl E. Robert, Rob van der Hilst, and Raymond Buland (1998). Global Teleseismic Earthquake Relocation with Improved Travel Times and Procedures for Depth Determination, Bulletin of the Seismological Society of America, Vol. 88, No. 3, pp. 722-743, June 1998.

Ferreira Ana M. G. and John H. Woodhouse (2007). Source, path and receiver effects on seismic surface waves, Geophysical Journal International, Vol. 168, Issue 1, pp. 109-132, doi: 10.1111/j.1365-246X.2006.03092.x

Gkika, F., Havskov, J., & Evangelidis, C. P. (2026). Teleseismic Data, Contribution from Greece. *Seismological Research Letters*, https://doi.org/10.1785/0220250254

Gkika F. and J. Havskov, November (2023). New Teleseismic Catalogue for NOA – Bridging the gap Report # 1 Preliminary results using data from 2019, Institute of Geodynamics - National Observatory of Athens Greece & Department of Geoscience University of Bergen Norway, Technical Report pp.37, http://www.geo.uib.no/seismo/REPORTS/GREECE/TELECAT_Report1_2023.pdf.

Gutenberg B. (1945). Amplitudes of surface waves and magnitudes of shallow earthquakes. Bulletin of Seismological Society of America, Vol. 35, no. 1, pp. 3–12. doi: 10.1785/BSSA0350010003.

Gutenberg B. (1945a). Amplitudes of P. PP. and S and magnitude of shallow earthquakes. Bulletin of Seismological Society of America, Vol 35, pp. 57–69.

Gutenberg B. (1945b). Magnitude determination of deep-focus earthquakes. Bulletin of Seismological Society of America, Vol. 35, pp. 117–130. Gutenberg B. and Richter C. F. (1956). Magnitude and energy of earthquakes. Annali di Geofisica, Vol. 9, no 1, pp. 1–15.

Gutenberg B. and Richter C. F. (1956). Magnitude and energy of earthquakes. Annali di Geofisica, Vol. 9, no 1, pp. 1–15.

Havskov. J. and K. Lieser (2021). Using ISC data. Summ. Bull. International Seismological Centre, January – June 2019, Vol. 56, no I, pp. 30–46, https://doi.org/10.31905/L2IR6ZNA.

Havskov. J., P. Voss and L. Ottemöller (2020). Seismological observatory software: Thirty years of SEISAN. Seismological Research Letters, Vol. 91, pp. 1846-1852.

Helmholtz-Centre Potsdam - GFZ German Research Centre for Geosciences and gempa GmbH. The SeisComP seismological software package. GFZ Data Services (2008). URL: https://www.seiscomp.de, doi:10.5880/GFZ.2.4.2020.003.

International Association of Seismology and Physics of the Earth's Interior (IASPEI) (2013). Summary of Magnitude Working Group recommendations on standard procedures for determining earthquake magnitudes from digital data, available at ftp://ftp.iaspei .org/pub/commissions/CSOI/Summary_WG_recommendations_20130327.pdf.

International Seismological Centre (2024). On-line Bulletin, https://doi.org/10.31905/D808B830 according to the International Registry of Seismograph Stations (International Seismological Centre, 2024b).

Jeffreys H. and K. E. Bullen (1967).Seismological Tables British Association for the Advancement of Science,Gray Milne Trust, London.

Kanamori, H., and Z. E. Ross (2019). Reviving mB, Geophys. J. Int., Vol. 216, pp. 1798–1816.

Kárník V., Kondorskaya N. V., Riznitchenko J. V., Savarensky E. F., Soloviev S. L., Shebalin N. V., Vanek J., and Zátopek A. (1962). Standardization of the earthquake magnitude scale. Stud. Geophys. Geodyn., Vol. 6, pp. 41–48. DOI: 10.1007/BF02590040.

Kennett B.L.N., Engdah E.R.and Buland R. (1995). Constraints on seismic velocities in the Earth from traveltimes. Geophys. J. Int., Vol 122, pp. 108-124.

Kennett B.L.N. and Engdahl E.R. (1991). Travel times for global earthquake location and phase association. Geophysical Journal International, Vol 105, pp. 429-465. DOI:10.17611/DP/9991809.

Ktenidou, O. J., Pikoulis, E. V., Papageorgiou, A., Gkika, F., Liakopoulos, S., Cekinmez, Z., ... & Evangelidis, C. P. (2026). The quest for reference stations at the National Observatory of Athens, Greece. Natural Hazards and Earth System Sciences, 26(1), 41-83.

Lienert B. and Havskov J. (1995). A Computer Program for Locating Earthquakes Both Locally and Globally. Seismological Research Letters, Vol 66, no5, pp. 26-36. DOI: 10.1785/gssrl.66.5.26. 37.

Lienert B. (1991). Report on modifications made to Hypocenter. Institute of Solid Earth Physics. University of Bergen.

Lienert B., Berg E., Frazer N. (1986). HYPOCENTER: An earthquake location method using centred, scaled and adaptively damped least squares. Bulletin of the Seismological Society of America, Vol 76, no 3, pp.771-783. DOI: 10.1785/BSSA0760030771.

Monthly Bulletins National Observatory of Athens - Geodynamic Institute, 1950-2002 (Available in print from the physical archive of GI/NOA).

Oliver J. and Murphy L. (1971). WWNSS: Seismology's global network of observing stations. Science, Vol. 174, pp. 254–261. doi: 10.1126/science.174.4006.254.

Peterson J. R. and Hutt C. R. (2014). World-wide standardized seismograph network: A data users guide. U.S. Geol. Surv., Open-File Report. 2014–1218, 74 pp. DOI: 10.3133/ofr20141218. Peterson J. R. (1993). Observation and modeling of seismic background noise. Open-File report 93-322, USGS, 95pp.

Selby Neil D., David Bowers, Peter D. Marshall and Alan Douglas (2003). Empirical path and station corrections for surface-wave magnitude, Ms, using a global network, Geophys. J. Int. (2003) 155, 379–390.

Stein, S. and Wysession, M. (2003). An Introduction to Seismology, Earthquakes, and Earth Structure, xi + 498 pp. Oxford: Blackwell Science, ISBN 0 865 42078 5.

Storchak D.A., J. Schweitzer and P. Bormann (2011). Seismic Phase Names: IASPEI Standard. In: Gupta H.K. (eds) Encyclopedia of Solid Earth Geophysics. Encyclopedia of Earth Sciences Series. Springer. Dordrecht. https://doi.org/10.1007/978-90-481-8702-7_11.

Storchak, D.A., J. Schweitzer, P. Bormann (2003). The IASPEI Standard Seismic Phase List, Seismol. Res. Lett., Vol. 74, no 6, pp. 761-772, https://doi.org/10.1785/gssrl.74.6.761.

Vaněk. J., Zapotek A., Karnik V., Kondorskaya N. V., Riznichenko Y. V., Savarensky E. F., Solov'yov S. L. and Shebalin N. V. (1962). Standarizaciya shkaly magnitude. Izvestiya Akad. SSSR. Ser. Geofiz. Vol. 2. pp. 153–158 (with English translation in 1962 by D. G. Frey. published in Izv. Geophys. Ser. (in Russian)).

APPENDIX I: *Average magnitude residuals per stations of HUSN for all type of magnitudes calculated, mB, mb, Ms and MS. Residuals were defined as the difference between the average event magnitude and the station magnitude. N is the number of station measurements; AV is the average magnitude residual and SD standard deviation. Reviewed data.*

Magnitude mb				**Magnitude mB**			**Magnitude Ms**			**Magnitude MS**		
STAT	N	AV	SD	N	AV	SD	N	AV	SD	N	AV	SD
AGG	21	-0.12	0.22	21	-0.12	0.12	28	0.03	0.07	29	0.04	0.06
ALN	29	-0.12	0.17	28	-0.05	0.12	35	-0.01	0.10	36	-0.03	0.11
AMPL	75	0.08	0.19	73	0.01	0.14	25	0.06	0.12	97	0.01	0.10
AMT	147	-0.03	0.17	146	-0.11	0.12	1	-0.03	0.00	169	-0.02	0.10
ANKY	291	0.05	0.22	287	0.07	0.13	39	-0.03	0.12	400	-0.01	0.13
ANX	296	-0.04	0.22	292	-0.11	0.15	44	-0.09	0.10	385	-0.08	0.09
AOS2	8	-0.14	0.22	8	-0.04	0.07	12	-0.06	0.06	14	-0.06	0.06
APE	220	-0.17	0.26	239	-0.10	0.16	43	-0.13	0.12	410	-0.11	0.12
ARG	302	0.26	0.23	313	0.17	0.17	46	-0.27	0.15	192	-0.26	0.15
ATAL	162	0.04	0.24	159	0.00	0.20	11	-0.01	0.10	206	-0.06	0.29
ATH	311	0.03	0.19	324	0.01	0.13	47	-0.09	0.10	481	-0.06	0.10
ATHU	310	-0.11	0.20	312	-0.09	0.14	35	-0.06	0.10	420	-0.07	0.17
AXAR	204	0.05	0.23	209	0.02	0.14	40	0.03	0.09	244	0.06	0.10
AXS	89	0.01	0.22	88	-0.02	0.12	33	0.01	0.11	96	0.04	0.32
CHOS	14	-0.05	0.13	14	0.02	0.07	21	-0.12	0.11	20	-0.12	0.10
CMBO	3	0.27	0.20	3	0.12	0.28	1	0.03	0.00	6	0.06	0.29
DION	200	0.12	0.31	213	0.15	0.24	38	0.05	0.19	234	0.17	0.23
DRO	282	0.15	0.23	297	0.13	0.14	40	-0.04	0.11	394	0.01	0.11
EFP	261	0.04	0.24	266	0.03	0.15	29	-0.01	0.11	273	0.02	0.10
EPID	144	-0.18	0.26	147	-0.13	0.13				144	-0.01	0.11
EVR	346	-0.02	0.26	342	-0.04	0.16	45	0.03	0.08	449	0.03	0.10
FNA	245	-0.12	0.24	249	-0.10	0.14	26	0.07	0.11	312	0.07	0.15
FSK	182	0.05	0.23	189	0.03	0.13	36	0.01	0.12	276	0.01	0.11
GRG	265	0.05	0.25	274	0.04	0.19	21	0.09	0.14	370	0.08	0.17
GUR	240	0.01	0.19	230	-0.04	0.13	39	-0.08	0.10	243	-0.06	0.11
GVD	297	0.08	0.22	315	0.11	0.12	42	-0.00	0.14	458	-0.01	0.14
HORT	303	-0.20	0.21	312	-0.13	0.12	46	0.06	0.11	424	0.04	0.14
IACM	192	0.43	0.26	180	0.22	0.22	31	-0.26	0.20	404	-0.11	0.17
IDI	296	-0.06	0.22	298	-0.05	0.14	43	-0.08	0.17	432	-0.08	0.16
IGT	270	-0.03	0.21	271	-0.02	0.11	44	0.06	0.11	381	0.07	0.11
IMMV	324	0.20	0.25	325	0.15	0.16	24	-0.07	0.14	442	-0.05	0.12
ITM	318	0.15	0.24	317	0.08	0.15	39	-0.05	0.08	434	-0.01	0.11
JAN	330	0.09	0.19	332	0.07	0.13	45	0.10	0.11	444	0.10	0.11
KALE	236	-0.07	0.19	239	-0.08	0.11	21	-0.04	0.12	271	0.01	0.10
KARP	302	0.25	0.29	302	0.21	0.20	41	-0.00	0.18	410	-0.02	0.16
KARY	179	-0.06	0.21	183	-0.01	0.11	14	0.01	0.13	215	0.01	0.13
KAVA	274	0.03	0.23	285	0.06	0.14	37	0.20	0.11	381	0.12	0.14

KEK	294	-0.02	0.22	304	-0.01	0.14	44	0.08	0.13	449	0.08	0.12
KLV	338	-0.04	0.22	336	-0.07	0.13	44	-0.06	0.11	462	-0.02	0.11
KNT	318	-0.03	0.20	316	0.02	0.14	32	0.63	0.15	262	0.07	0.19
KOKK	89	-0.12	0.19	92	-0.07	0.11	25	-0.03	0.08	116	-0.03	0.10
KPRO	220	-0.06	0.33	218	-0.05	0.21	21	0.05	0.11	324	0.02	0.24
KRND	157	-0.13	0.21	163	-0.10	0.15	24	-0.04	0.11	240	-0.04	0.09
KSL	225	0.04	0.26	233	0.02	0.16	42	0.06	0.12	374	0.04	0.12
KSTE	4	0.41	0.22	4	0.18	0.13				5	0.06	0.15
KTHA	149	0.07	0.20	154	0.08	0.10	21	-0.06	0.07	253	-0.02	0.11
KZN	309	-0.13	0.25	309	-0.10	0.14	39	0.08	0.24	452	0.07	0.13
LAKA	230	-0.08	0.21	234	-0.04	0.10				339	-0.00	0.16
LIA	287	-0.07	0.32	306	-0.06	0.24	39	0.14	0.22	424	-0.07	0.23
LIT	270	0.00	0.25	275	0.02	0.16	28	0.01	0.09	366	0.03	0.11
LKD2	292	0.05	0.22	294	0.09	0.11	41	0.04	0.11	423	0.06	0.14
LKR	306	-0.02	0.23	305	-0.05	0.14	43	0.01	0.09	278	0.01	0.10
LOUT	192	-0.09	0.19	191	-0.11	0.11	21	-0.07	0.09	191	-0.01	0.09
LTHK	130	0.05	0.22	128	0.02	0.14	40	0.03	0.11	170	0.07	0.12
LTK	235	-0.14	0.22	239	-0.13	0.15	35	-0.06	0.08	356	-0.05	0.09
MDRA	33	-0.29	0.23	31	-0.22	0.18				14	-0.03	0.08
MRKA	63	-0.00	0.19	62	-0.01	0.12				62	0.04	0.11
NEO	310	-0.02	0.24	319	-0.00	0.15	45	-0.04	0.09	467	-0.02	0.10
NEST	262	-0.05	0.27	266	-0.06	0.16	41	0.04	0.13	396	0.05	0.12
NIS1	70	0.09	0.22	75	0.02	0.14				124	-0.10	0.13
NPS	229	0.10	0.23	225	0.07	0.15	13	-0.04	0.20	315	-0.03	0.17
NVR	308	-0.07	0.22	312	-0.04	0.13	14	0.03	0.10	435	0.06	0.13
OUR	300	-0.02	0.21	317	0.01	0.10	44	-0.03	0.10	425	-0.03	0.09
PAIG	260	-0.04	0.27	259	-0.03	0.21	18	-0.01	0.08	360	-0.08	0.19
PDO	181	0.07	0.22	186	0.06	0.12	10	0.06	0.12	210	0.07	0.20
PENT	281	-0.10	0.26	284	-0.03	0.15	26	0.13	0.18	227	0.12	0.13
PLEV	48	0.04	0.16	46	0.02	0.10				58	0.07	0.08
PLG	264	0.04	0.23	265	0.04	0.15	23	0.14	0.12	283	0.10	0.21
PRAS	19	-0.03	0.24	19	-0.02	0.15				21	0.04	0.14
PRK	318	0.09	0.21	323	0.03	0.13	39	-0.04	0.09	465	-0.06	0.10
PRMD	55	0.17	0.23	56	0.16	0.14	15	0.02	0.07	79	0.01	0.09
PTL	295	0.03	0.23	307	0.01	0.13	42	-0.03	0.11	396	0.01	0.09
PVO	219	0.05	0.26	231	0.11	0.17	36	0.11	0.14	322	0.11	0.16
PYL	283	0.04	0.19	283	0.03	0.13	11	0.01	0.13	385	-0.01	0.12
RDO	275	-0.08	0.23	278	-0.05	0.17	43	0.00	0.12	394	-0.01	0.25
RLS	323	0.16	0.24	331	0.13	0.16	35	0.09	0.11	337	0.07	0.11
SERG	112	-0.10	0.21	112	-0.10	0.13	44	-0.03	0.08	144	-0.01	0.09
SERI	116	-0.18	0.25	129	-0.14	0.14				126	-0.11	0.09
SIGR	267	-0.02	0.23	287	-0.01	0.12	47	-0.05	0.10	439	-0.06	0.10
SIVA	205	0.18	0.22	204	0.14	0.15				268	-0.07	0.19
SKY	194	0.12	0.24	211	0.12	0.14	42	0.03	0.10	375	0.03	0.09

SMG	262	-0.00	0.26	277	0.00	0.14	31	-0.06	0.12	427	-0.08	0.11
SMTH	305	-0.19	0.23	323	-0.13	0.13	47	-0.03	0.10	459	-0.04	0.11
SRS	318	-0.08	0.21	330	-0.03	0.11	41	0.03	0.12	463	0.03	0.14
TETR	85	0.23	0.24	88	0.17	0.14	32	0.07	0.10	100	0.03	0.11
THAL	180	0.04	0.19	177	-0.02	0.13				164	-0.04	0.10
THAS	229	-0.11	0.23	236	-0.07	0.13	40	-0.04	0.10	372	-0.05	0.09
THE	320	-0.18	0.22	323	-0.14	0.12	23	0.09	0.16	362	0.07	0.15
THERA	15	0.07	0.22	15	0.03	0.16	22	-0.17	0.14	20	-0.18	0.13
THL	313	-0.28	0.27	322	-0.19	0.14	45	0.03	0.10	484	0.03	0.11
VAM	222	0.17	0.23	216	0.16	0.15	7	0.05	0.15	333	0.01	0.15
VILL	291	-0.14	0.20	292	-0.10	0.11	21	-0.05	0.10	254	-0.05	0.09
VLI	300	0.03	0.25	298	0.03	0.17	41	0.12	0.09	413	0.08	0.15
VLS	270	0.02	0.27	259	0.03	0.14	46	0.01	0.12	407	0.03	0.10
VLX	232	-0.15	0.23	228	-0.11	0.16	31	-0.13	0.11	255	-0.05	0.12
VLY	306	-0.03	0.20	310	-0.03	0.13	47	-0.10	0.10	471	-0.06	0.10
VVK	96	0.11	0.24	98	0.06	0.13	34	-0.06	0.11	103	-0.04	0.10
XOR	236	-0.02	0.32	240	-0.02	0.28	12	-0.16	0.26	329	-0.05	0.22
ZKR	261	0.16	0.23	262	0.10	0.17	42	-0.00	0.16	408	0.01	0.15

APPENDIX II

Special cases

The following cases illustrate challenges revealed during the analysis and are discussed separately.

Case 1 Overlapping events

Event near the coast of central Chile on September 16, 2015. Origin time 22:54:30.6, Lat -31.641, Long -71.689, with magnitude of Mb 7.0 and Ms 8.0 and depth 12.1 Km (ISC). Distance from ATH station of the network approximately center and the hypocenter is 12516 Km.

This earthquake had several aftershocks within the first half hour following the main shock, Figure 14. The details of these events are as follows:

First event: Origin time 22:59:12.0, Magnitude Mb 6.4

Second event: Origin time 23:03:55.6, Magnitude Mb 6.0

Third event: Origin time 23:16:07.5, Magnitude Mb 6.0

Fourth event: Origin time 23:18:41.3, Magnitude Mb 6.4 and MS 7.2

The signals of all these aftershocks were mixed with the signals of the main shock, which was recorded for more than two hours. Only the first P arrival of the main shock was picked and identified as Pdif. While the phases of the aftershocks could not be identified. In addition to the first arrival of the main shock, the surface wave amplitudes were also read assuming that the large amplitude surface waves are associated with the main shock

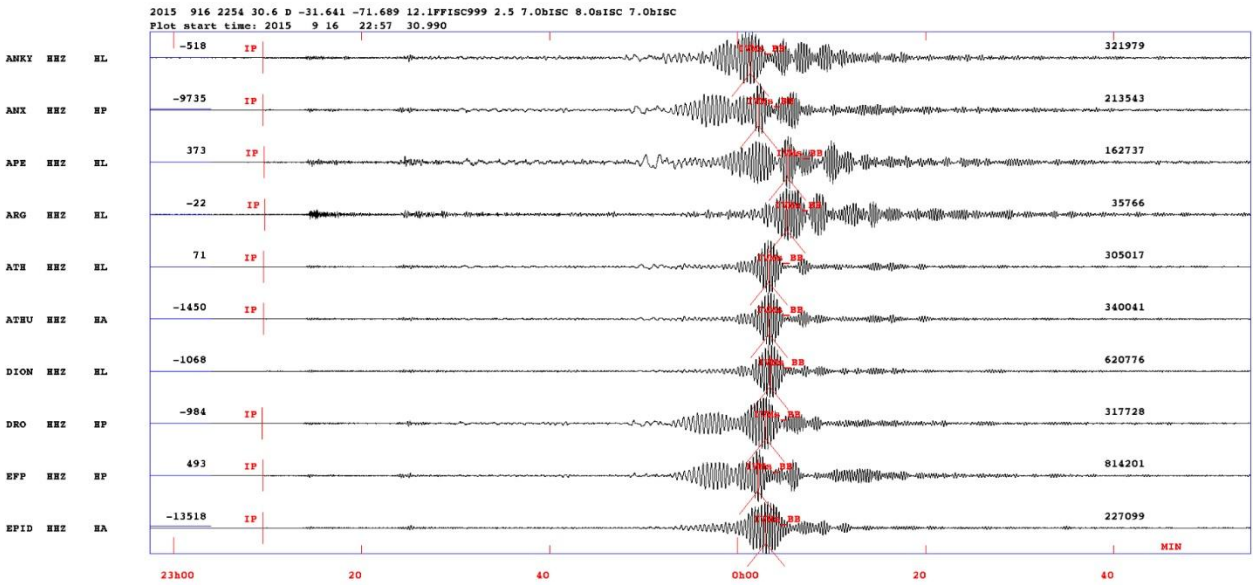

Figure 14: Event near the coast of central Chile on 20150916, origin time 22:54:30.6, Lat -31.641, Long -71.689, Depth 12.1 Km, magnitude Mb 7.0 and Ms 8.0 (ISC prime solution).

Case 2 Two events at the same origin time but at different locations

On January 14, 2016, our database contains two significant events that occurred almost simultaneously, with only a six-second difference in their origin times and distinct hypocenters. The first event is a deep event with 582 Km depth, located at Bolivia with origin time at 03:25:27.6 and magnitude Mb 6.0 according to the ISC prime solutions. The other event following the Bolivia event in our database, is located at Hokkaido with origin time 03:25:33.6 it is an event with depth 54.9 Km and magnitude Mb 6.5 (ISC).

Bolivia event has a distance of 11084 Km from ATH station that is located approximately in the center of the network and arrives almost 11 sec after the arrival of Hokkaido event based on the theoretical phases of the event (fixed), Figure 15.

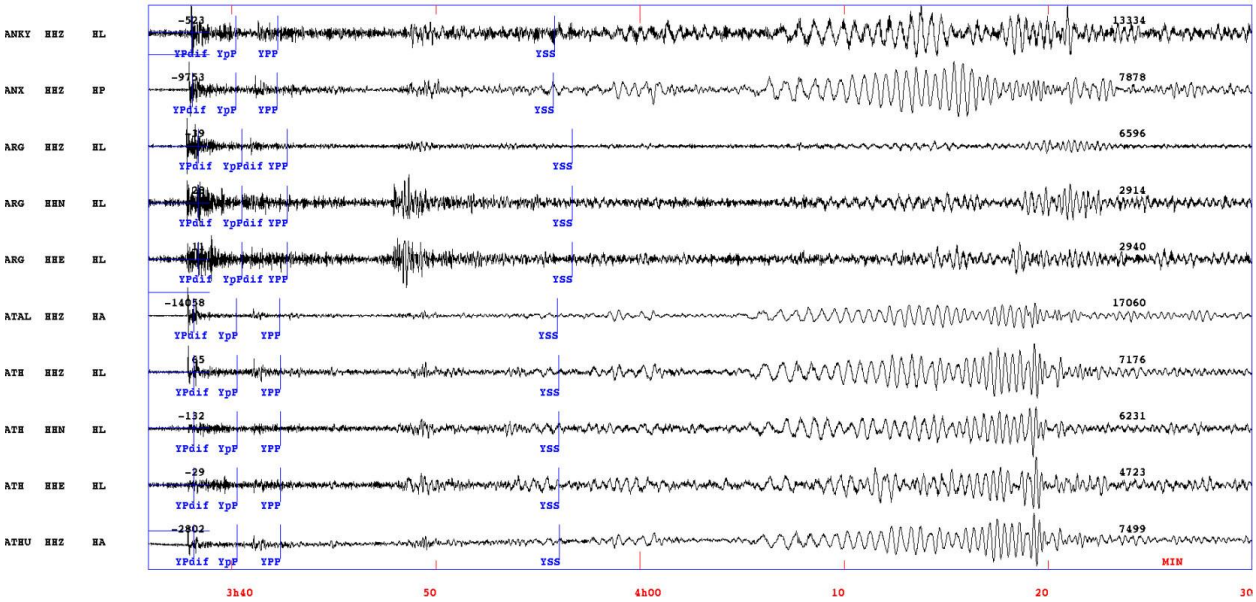

Figure 15: Event at Bolivia on 20160114 origin time 03:25:27.6, Lat -19.711, Lon -63.317, Depth 582 Km, magnitude Mb 6.0 (ISC prime solution). Blue lines describe the theoretical arrival times (IASP) of different phase types of the Bolivia event, which arrives later with respect to Hokkaido event. Japan event as bigger magnitude and closer distance dominates and the phase's arrivals of Bolivia event cannot be distinguished.

Hokkaido event, which occurs at closer distance from ATH station, 9.215 Km, arrives first in the network stations. It dominates in the recordings since it is larger and different phase's arrivals can be clearly detected, Figure 16. Since Bolivia event is smaller, it cannot be seen in Japan trace.

In cases of two events, with similar origin times, the importance of theoretical phases (IASP) arises, must always be taken into consideration.

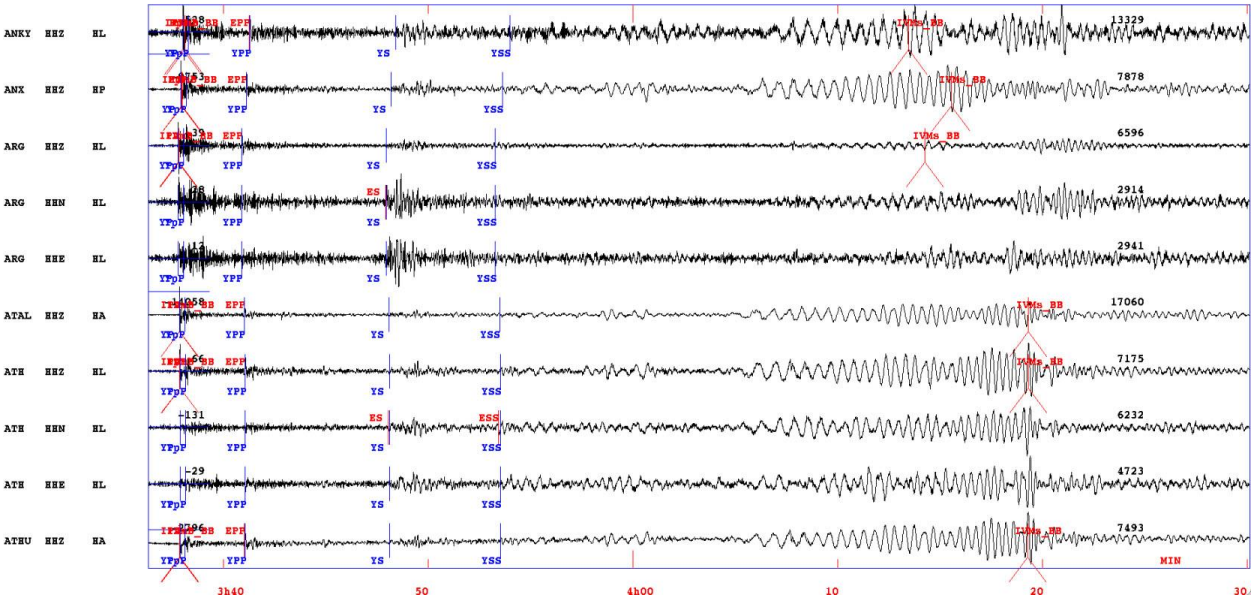

Figure 16: Hokkaido event at 20160114, origin time 03:25:33.6, Lat 42.044, Lon 142.697, Depth 54.9 Km and magnitude Mb 6.5 & Ms 6.3 (ISC prime solution).

Difficult phase identification at large distances

Case 3 mixing PKPdf and Pdif

Event on December 8, 2016, located at Bougainville-Solomon Islands region. Origin time 173846.8, Lat -10.790, Long 161.280, with magnitudes Mb 7.1 and Ms 8.3 and depth of 47.6 Km (ISC prime solution). Distance of the hypocenter from ATH station is 14848 Km.

The travel time of Pdif and PKPdf can be very similar at some large distances, Figure 17. Since the phases are read as P and the program tries to find the most correct first arrival a slightly wrong distance might misidentify the first arrival and the user will have to assign the correct one. This can particularly be a problem with a relatively small network like the Greek network. More global stations would help.

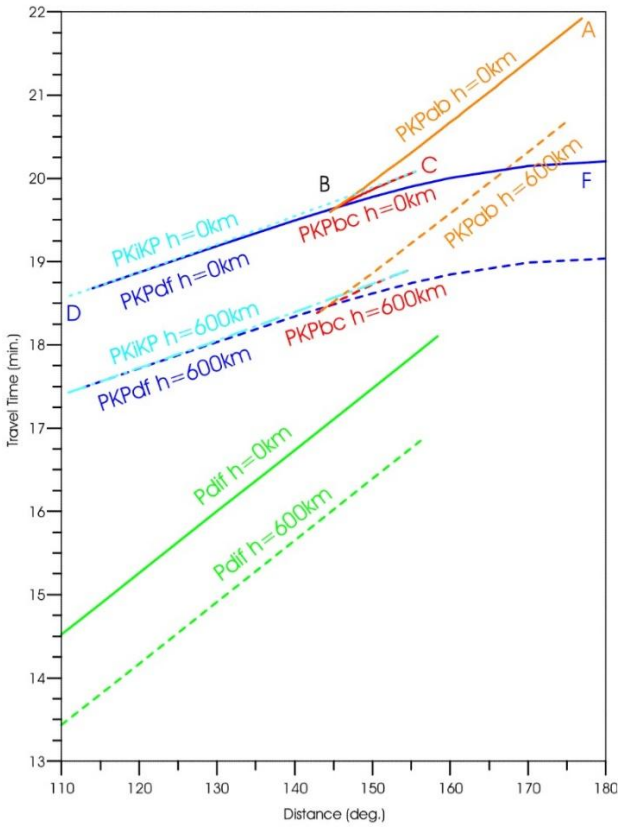

Figure 17: Travel time curves of Pdif and PKP phases by IASP91 for surface and deep events, (Bormann, 2012).

In this event a case like this is presented, where picking the first arriving phases as simple P and trying to locate, the program identifies the first arrival as PKPdf resulting in a bad location. This can be seen in the produced high residuals in the location process and can be solved easily if the first arriving phases are changed in the S-file from P to Pdif and then locating the event, Figure 18**Error! Reference source not found.**. In cases like this apart from the accuracy of the phase arrival and depending on the distance and the depth of the event processed, the user should be able to know what to expect and interfere in the S-file pushing the program to the correct identification. The theoretical phases arrivals (IASP) available in the program gives correct identifications of Pdif and PKPdf. Furthermore, due to the numerus phases arrivals at different teleseismic distances travel time diagrams of body waves could? be advised (Jeffreys and Bullen (1967), see Stein and Wysession, (2003)).

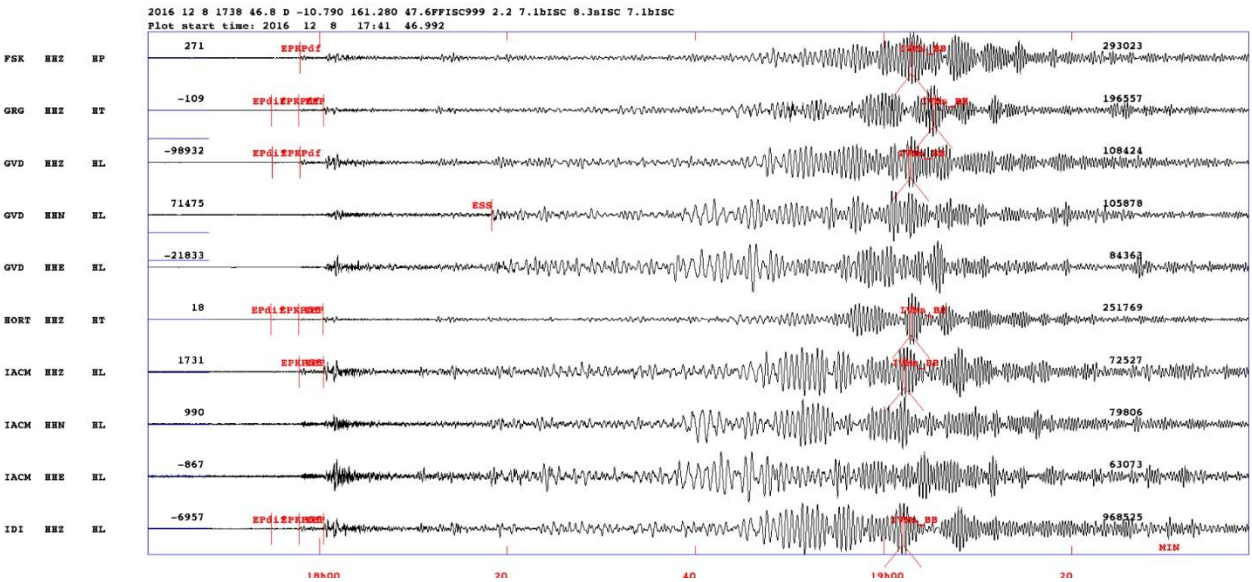

Figure 18: Event at Bougainville-Solomon Islands region 20161208, origin time 17:38:46.08, Lat -10.790, Long 161.280 , Depth 47.6, magnitudes Mb 7.1 and Ms 8.3 (ISC prime solution).

This was a great event of magnitude Ms 8.3 and many phases could be recognized such as Pdif, PKPdf, pPKPdf, PP and SS. Every phase's arrival could be detected with clear change in the waveforms but their exact arrival during picking could be approached with not so much accuracy, Table 9. As can be seen from the location results higher residuals are present, it was decided to keep all this valuable information for this event, unaffected by the residuals.

Table 9:

date	hrmn	sec	lat	long	depth	no	m	rms	damp	erln	erlt	erdp	
1612	8 1738	44.63	1047.40S	161 16.8E	47.6	190	2	3.61	0.000207.8224.7		0.0		
stn	dist	azm	ain	w	phas	calcphs	hrmn	tsec	t-obs	t-cal	res	wt	di
KSL	14432	308.3	18.7	0	Pdif	Pdif	1754	37.9	953.27	951.37	1.89	1.00	1 HL
KSL	14432	308.3	28.1	0	PP	PP	18 0	6.21281.611274.59			7.02	1.00	2 HL
KSL	14432	308.3	7.8	0	PKPdf	PKPdf	1757	49.21144.541143.43			1.11	1.00	0 HL
ARG	14554	308.8	27.9	0	PP	PP	18 0	8.91284.301281.74			2.55	1.00	1 HL
ARG	14554	308.8	7.8	0	PKPdf	PKPdf	1757	52.51147.881145.51			2.37	1.00	0 HL
RDO	14559	315.9	18.7	0	Pdif	Pdif	1754	42.2	957.58	956.42	1.15	1.00	0 HL
RDO	14559	315.9	7.8	0	PKPdf	PKPdf	1757	44.11139.501145.57			-6.07	1.00	0 HL
PRK	14587	313.3	18.7	0	Pdif	Pdif	1754	41.1	956.50	957.57	-1.07	1.00	0 HL
PRK	14587	313.3	7.8	0	PKPdf	PKPdf	1757	45.01140.341146.05			-5.72	1.00	0 HL

Case 4: mixing Pdif and pPdif

Surface event on July 30, 2021 located at Minahassa Peninsula, Sulawesi. Origin time 17:10:18.00 with Lat -5.003 and Long -80.696, depth 34.3 Km and magnitude of Mb 6.3 (ISC). The closest station from the network to the hypocenter is IGT at 11318 Km.

In this event, first arrivals are Pdif according to the theoretical arrivals but these are clearly seen only in a few stations because there is a low signal to noise ratio, Figure 20 and Figure 21. Therefore, if reading the first arrival as P, the program will identify it as Pdif while in reality it is pPdif, Figure 19. The Pdif will have small arrivals since Pdif and pPdif are close together and only a few stations is used (Tabel 10). The Pdif is seen in some trace as a weak arrival before the first clear arrival. In this case the users must choose to identify the first arrival as pPdif.

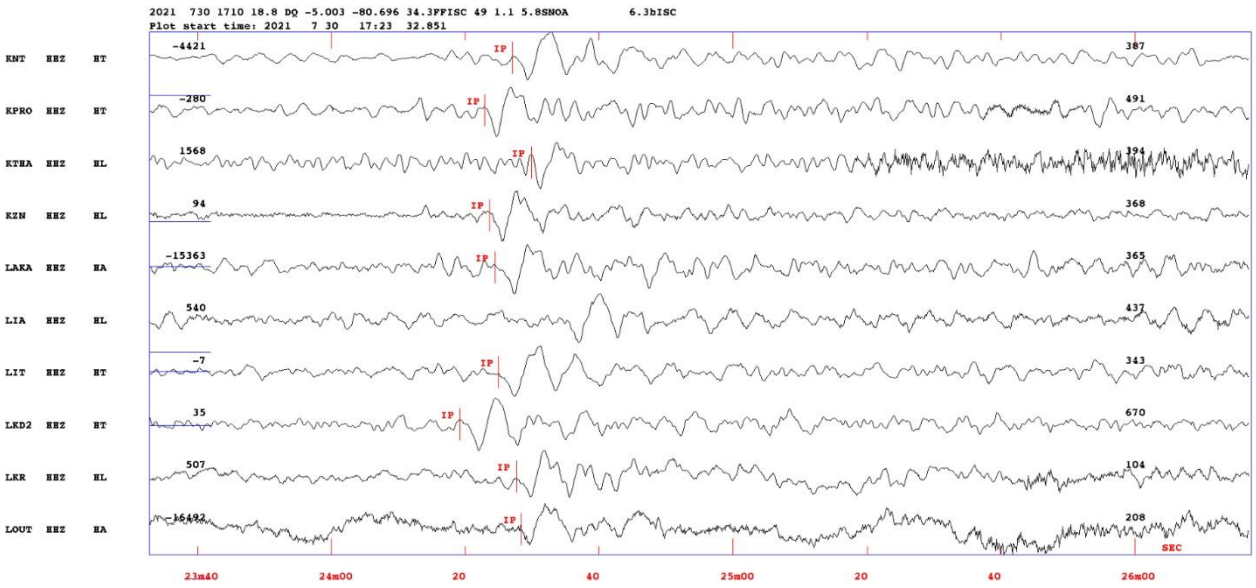

Figure 19: Surface Event located at Minahassa Peninsula, Sulawesi, on 20210730, origin time 17:10:18.00, Lat -5.003, Long -80.696, Depth 34.3 Km, magnitude Mb 6.3 (ISC prime solution). First picking with simple P on the pPdif phase arrival.

Table 10: Surface Event at 30072021 origin time 17:10:18.00 located at Minahassa Peninsula, Sulawesi with Lat -5.003 and Long -80.696, magnitude Mb 6.3 depth 34.3 Km (ISC).Location results with first picking with simple P on the pPdif phase arrival wrong phase identification as Pdif.

date	hrmn	sec	lat	long	depth	no	m	rms	damp	erln	erlt	erdp	
21	730	1710	29.86	5 0.18S	80 41.8W	34.3		39	2	0.58	0.000	999.9	999.9	0.0	
stn	dist	azm	ain	w	phas	calcphs	hrmn	tsec	t-obs	t-cal	res	wt	di		
IGT	11318	50.8	15.0	0	P	Pdif	1724	18.3	828.46	828.76	-0.30	1.00	1	HT	
FSK	11344	51.9	15.0	0	P	Pdif	1724	19.7	829.80	829.78	0.02	1.00	1	HP	
VLS	11348	52.2	15.0	0	P	Pdif	1724	19.6	829.78	829.98	-0.21	1.00	1	HL	
LKD2	11351	51.6	15.0	0	P	Pdif	1724	19.2	829.29	830.09	-0.81	1.00	1	HT	
JAN	11362	50.7	15.0	0	P	Pdif	1724	21.0	831.15	830.54	0.61	1.00	1	HL	
PENT	11382	50.1	15.0	0	P	Pdif	1724	21.6	831.75	831.46	0.29	1.00	1	HL	
AMPL	11398	51.4	15.0	0	P	Pdif	1724	22.3	832.49	831.94	0.54	1.00	1	HP	
TETR	11400	51.0	15.0	0	P	Pdif	1724	23.1	833.23	832.15	1.08	1.00	1	HL	
2021	730	1710	29.9	DQ	-5.003	-80.696	34.3	FFISC	39	0.6				6.3bISC	

```
OLD: 0730 1710 18.8 DQ -5.003 -80.696 34.3FFISC 49 1.1 5.8SNOA          6.3bISC
```

If the above notice is omitted and the picking continues, adding more later arriving clear phases such as SKSac (picked as simple S) and then relocating, the identification of the extra phases will be correct as SKSac but with unjustified high residuals, of the order of -14 sec. This problem will be solved if pPdif phase is originally picked not as simple P phase but as pP or pPdif then with the location process the code will recognize it correctly as pPdif, Figure 20. See in the final solution all phases residuals are logical and low, Table 11.

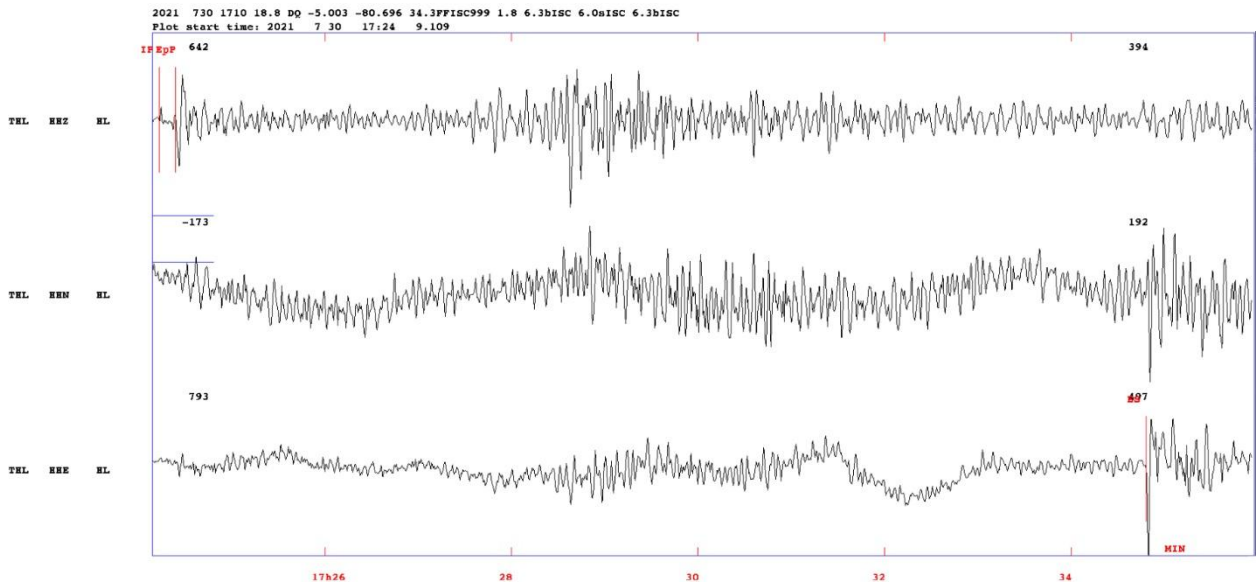

Figure 20: Surface Event located at Minahassa Peninsula, Sulawesi, on 20210730, origin time 17:10:18.00, Lat -5.003, Long -80.696, Depth 34.3 Km, magnitude Mb 6.3 (ISC prime solution). Three-component station THL, first phase arrival Pdif picked as simple P secondary phase pPdif picked as pP and SKSac picked as simple S.

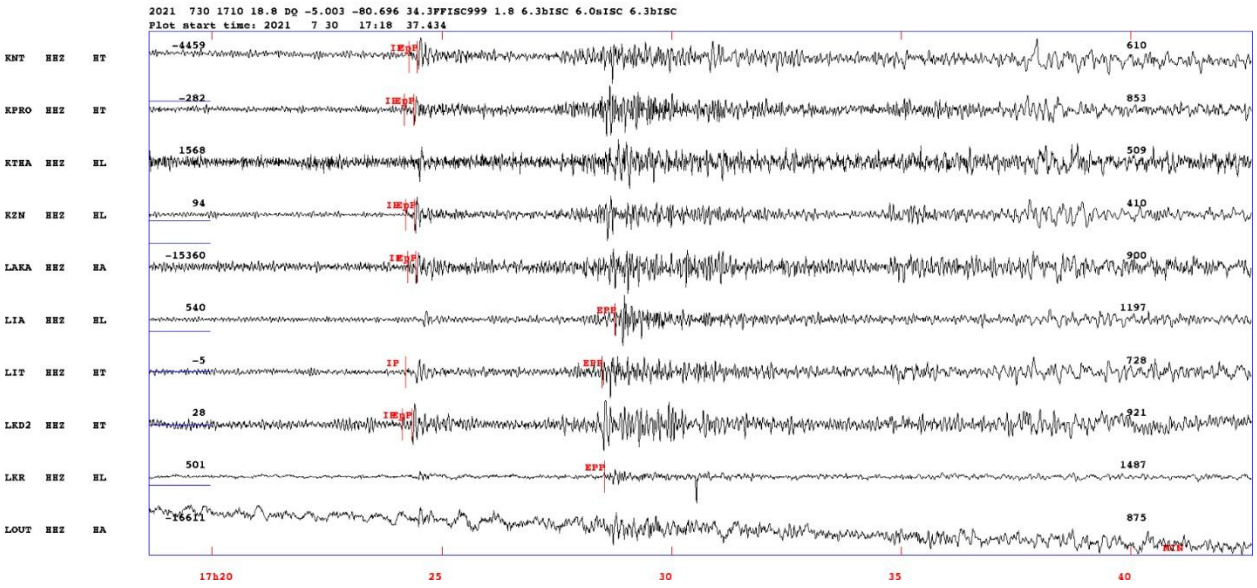

Figure 21: Surface Event located at Minahassa Peninsula, Sulawesi, on 20210730, origin time 17:10:18.00, Lat -5.003, Long -80.696, Depth 34.3 Km, magnitude Mb 6.3 (ISC prime solution). Phases picked at several stations.

Table 11: Event on 30072021 171018.08 Lat -5.003 Long -80.696 magnitude Mb 6.3 depth 34.3 Km. Abbreviations in the solution of the event describe Date, origin time, latitude, Longitude, Depth, rms.

date	hrmn	sec	lat	long	depth	no	m	rms	damp	erln	erlt	erdp
21	730	1710	18.78	5 0.18S	80 41.8W	34.3		88	2	1.14	0.000	186.2	219.8	0.0

stn	dist	azm	ain	w	phas	calcphs	hrmn	tsec	t-obs	t-cal	res	wt	di	
IGT	11318	50.8	15.0	0	P	Pdif	1724	8.2	829.38	828.76	0.62	1.00	0	HT
IGT	11318	50.8	165.0	0	pP	pPdif	1724	18.5	839.71	839.72	-0.01	1.00	0	HT
VLS	11348	52.2	9.2	0	S	SKSac	1734	43.7	1464.9	2146	6.66	-1.74	1.00	0 HL
VLS	11348	52.2	15.0	0	P	Pdif	1724	8.6	829.80	829.98	-0.18	1.00	0	HL
VLS	11348	52.2	165.0	0	pP	pPdif	1724	19.4	840.67	840.94	-0.27	1.00	0	HL
LKD2	11351	51.6	15.0	0	P	Pdif	1724	7.7	828.96	830.09	-1.13	1.00	0	HT
LKD2	11351	51.6	165.0	0	pP	pPdif	1724	20.1	841.32	841.05	0.27	1.00	0	HT
AMPL	11398	51.4	15.0	0	P	Pdif	1724	11.9	833.17	831.94	1.23	1.00	0	HP
AMPL	11398	51.4	165.0	0	pP	pPdif	1724	22.3	843.57	842.90	0.67	1.00	0	HP

Concluding: When working with teleseismic it is useful to fix solution to an agency that has a global network, this way special cases like overlapping events will be distinguished. High residuals usually depict wrong phase name identification when locating. IASP theoretical arrivals needs to be advised. There always be cases that the user will have to interfere in the phase name identification.

APPENDIX III: Magnitude ML residuals check

In addition to examining the magnitude mb, mB and MS residuals of KARY station from the teleseismic database, the ML (Local magnitude) of KARY station residuals were also analyzed using the local seismicity database of GI-NOA. For a part of the problematic time period examined, it was observed that the ML residuals were low and potentially misleading. The dataset used consisted of events with ML >=2.5 period 2012/01/01-2013/06/31, approximately 5063 events. The results for the station's horizontal components were as follows: HHE had an average residual of -0.14, and HHN had an average residual of -0.13. These average residuals were derived from only 56 readings, indicating a small number of ML readings for this station compared to the large dataset used, indicating that the station was not used in magnitude readings for higher magnitude events probable cause of large residuals.

Keeping in mind that stations with outlying magnitudes might be excluded in daily analyses of local seismicity. This observation was further confirmed by making a few ML readings on KARY station selecting events with magnitudes greater than 4 during that period. For the events magnitude readings of KARY station were not included in the solutions, **Error! Reference source not found.**Appendix III. As can be seen large residuals starts to be formed that comes in agreement that the station had a response problem during that period. This is mentioned cause the response issue of KARY could not be detected by just plotting ML residuals over time cause the database was incomplete in ML magnitude readings for this station.

Table Appendix III: ML is the event Local magnitude reported from NOA. Refers to the average of 2 horizontals comps MLh. KARY ML is the magnitude reading at the named station. KARY ML res is the residual derived from the difference of the event magnitude and the magnitude reported at the named station.

Date	*Time*	*ML*	*KARY ML*	*KARY ML res*
10/6/2012	*12:44*	*5,8*	*6,58*	*0,78*
10/6/2012	*12:49*	*5*	*5,58*	*0,58*
9/7/2012	*13:54*	*5,4*	*5,95*	*0,55*
6/8/2012	*15:22*	*4,1*	*4,75*	*0,65*
9/9/2012	*7:26*	*4,2*	*5,03*	*0,83*
27/1/2012	*1:33*	*5,2*	*5,9*	*0,7*
			AVERAGE	***0,68***

Concluding when investigating station discrepancies in terms of magnitudes it is important that all readings must be kept in order to have a complete database. A solution for the outlying readings is to be kept inactive and so not contributing in the events magnitude calculation.